NASA TechBriefs

National Aeronautics and
Space Administration


Electronic Components and Circuits


Electronic Systems


Physical Sciences


Materials


Computer Programs


Mechanics


Machinery


Fabrication Technology


Mathematics and Information Sciences


Life Sciences

March 2002

INTRODUCTION

Tech Briefs are short announcements of innovations originating from research and development activities of the National Aeronautics and Space Administration. They emphasize information considered likely to be transferable across industrial, regional, or disciplinary lines and are issued to encourage commercial application.

Availability of NASA Tech Briefs and TSPs

Requests for individual Tech Briefs or for Technical Support Packages (TSPs) announced herein should be addressed to

National Technology Transfer Center
Telephone No. **(800) 678-6882** or via World Wide Web at **www2.nttc.edu/leads/**

Please reference the control numbers appearing at the end of each Tech Brief. Information on NASA's Commercial Technology Team, its documents, and services is also available at the same facility or on the World Wide Web at **www.nctn.hq.nasa.gov**.

Commercial Technology Offices and Patent Counsels are located at NASA field centers to provide technology-transfer access to industrial users. Inquiries can be made by contacting NASA field centers and program offices listed below.

NASA Field Centers and Program Offices

Ames Research Center
Carolina Blake
(650) 604-1754 or
cblake@mail.arc.nasa.gov

Dryden Flight Research Center
Jenny Baer-Riedhart
(661) 276-3689 or
jenny.baer-riedhart@dfrc.nasa.gov

Goddard Space Flight Center
George Alcorn
(301) 286-5810 or
galcorn@gsfc.nasa.gov

Jet Propulsion Laboratory
Merle McKenzie
(818) 354-2577 or
merle.mckenzie@jpl.nasa.gov

Johnson Space Center
Hank Davis
(281) 483-0474 or
henry.l.davis1@jsc.nasa.gov

John F. Kennedy Space Center
Jim Aliberti
(321) 867-6224 or
Jim.Aliberti-1@ksc.nasa.gov

Langley Research Center
Sam Morello
(757) 864-6005 or
s.a.morello@larc.nasa.gov

Glenn Research Center
Larry Viterna
(216) 433-3484 or
cto@grc.nasa.gov

George C. Marshall Space Flight Center
Vernotto C. McMillan
(256) 544-2615 or
vernotto.mcmillan@msfc.nasa.gov

John C. Stennis Space Center
Kirk Sharp
(228) 688-1929 or
technology@ssc.nasa.gov

NASA Program Offices
At NASA Headquarters there are seven major program offices that develop and oversee technology projects of potential interest to industry:

Carl Ray
Small Business Innovation Research Program (SBIR) & Small Business Technology Transfer Program (STTR)
(202) 358-4652 or
cray@mail.hq.nasa.gov

Dr. Robert Norwood
Office of Commercial Technology (Code RW)
(202) 358-2320 or
rnorwood@mail.hq.nasa.gov

John Mankins
Office of Space Flight (Code MP)
(202) 358-4659 or
jmankins@mail.hq.nasa.gov

Terry Hertz
Office of Aero-Space Technology (Code RS)
(202) 358-4636 or
thertz@mail.hq.nasa.gov

Glen Mucklow
Office of Space Sciences (Code SM)
(202) 358-2235 or
gmucklow@mail.hq.nasa.gov

Roger Crouch
Office of Microgravity Science Applications (Code U)
(202) 358-0689 or
rcrouch@hq.nasa.gov

Granville Paules
Office of Mission to Planet Earth (Code Y)
(202) 358-0706 or
gpaules@mtpe.hq.nasa.gov

NASA TechBriefs

National Aeronautics and
Space Administration

March 2002
02-03

5 Electronic Components and Circuits

11 Electronic Systems

19 Physical Sciences

31 Materials

35 Computer Programs

41 Mechanics

47 Machinery

51 Fabrication Technology

57 Mathematics and Information Sciences

61 Life Sciences

4

BLANK PAGE

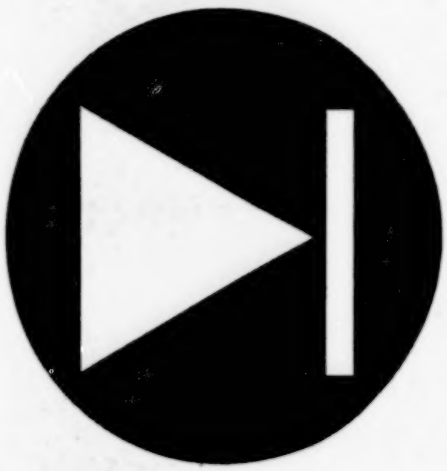

Electronic Components and Circuits

Hardware, Techniques, and Processes

7 Mounting Flip Chips on Heat-Dissipating, Matched-CTE Boards
8 Lightweight, Dimensionally Stable Printed-Wiring Boards
8 Nanoelectronic Devices With Precise Atomic-Scale Structures

Books and Reports

10 PCI Bridge to Instruments and Telecommunication Systems

BLANK PAGE

Mounting Flip Chips on Heat-Dissipating, Matched-CTE Boards

Integrated-circuit chips can run cooler, and solder joints are less likely to fail.

John H. Glenn Research Center, Cleveland, Ohio

"Flip chip on board (FCOB) with high thermal conductivity and tailored coefficient of thermal expansion (CTE)" denotes a developmental concept for relatively inexpensive, lightweight packaging of electronic circuits to accommodate high densities of components and of interconnections. The concept addresses several issues that pertain to flip-chip performance and reliability and to the integration of flip chips with other components: These issues include minimization of undesired mismatches of CTEs between flip chips and printed-wiring boards (PWBs), removal of heat from high-power flip chips, and the need to maximize stiffness while minimizing weight.

Usually, a conventional PWB is made of an epoxy-matrix/glass-fiber laminate, called "FR-4," with copper surface layers that can be etched to form signal and power conductors. A PWB of the present developmental type includes a core layer that contains a carbon cloth, sandwiched between FR-4 outer layers. Typically, the thickness of the carbon-cloth layer is about one-third the overall thickness of the laminate.

Carbon cloth is used in the core layer because it has several properties that are desirable with respect to the issues mentioned above. These properties include the high thermal conductivity of carbon fibers (up to 1,100 W/m·K), low CTE [$<<10^{-6}$ $(°C)^{-1}$ in some cases], low mass density [≈0.07 $lb/in.^3$ (1.9 kg/m^3) for carbon versus ≈0.1 $lb/in.^3$ (2.8 kg/m^3) for aluminum], and high stiffness [up to ≈42 Mpsi (≈290 GPa) for carbon versus ≈10 Mpsi (≈69 GPa) for aluminum].

The use of a carbon-fiber core layer to increase the thermal conductance of a PWB and thus the ability of the PWB to dissipate heat offers two benefits. One benefit is higher reliability: It has been estimated that in many cases, lowering the temperature of operation of electronic components by 10 °C approximately doubles the mean time between failures of the components. The other benefit is that lower operating temperatures enable components (especially data processors) to function at greater speeds and efficiencies.

Thus far, thermal testing of specimens and finite-element modeling of carbon-fiber-core FCOBs have shown the potential for matching of CTEs and lowering operating temperatures of components. In one example in the temperature analysis (see figure), the peak temperature under a flip chip was estimated to be ≈277 °F (≈136 °C) on a conventional FR-4 PWB but only ≈129 °F (≈54 °C) on a carbon-fiber-core PWB.

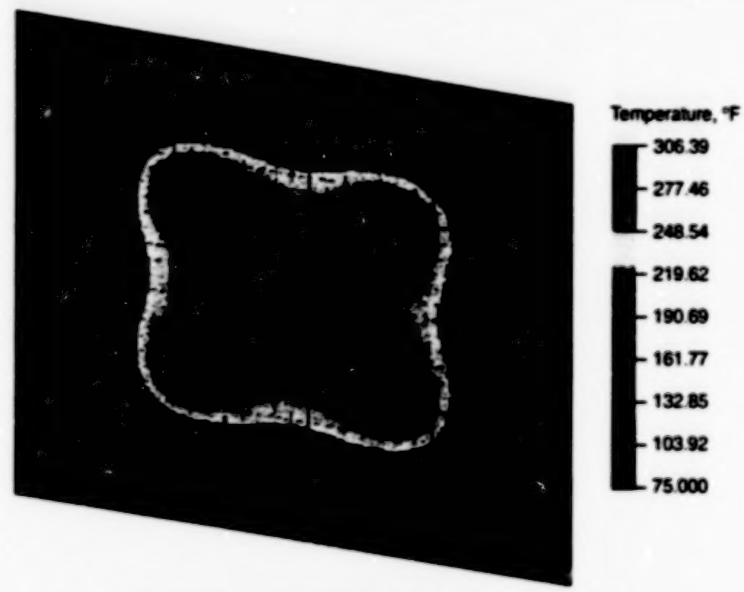

TEMPERATURE MAP FOR CONVENTIONAL PWB

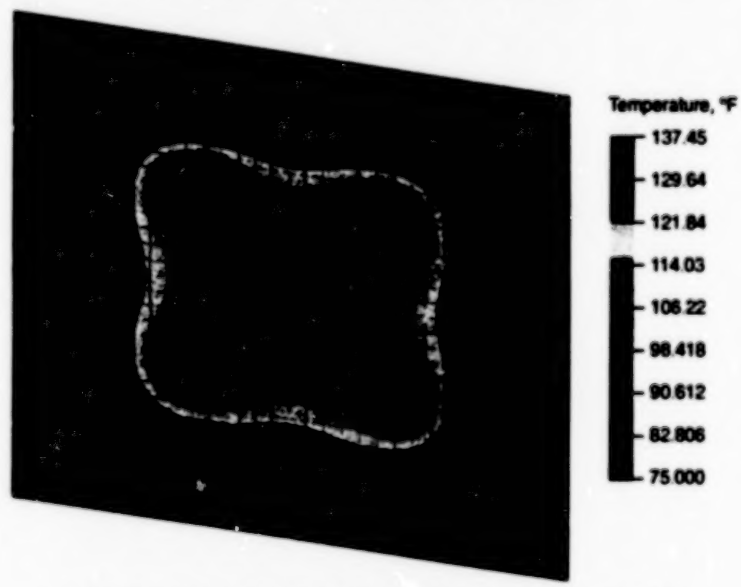

TEMPERATURE MAP FOR PWB WITH CARBON-FIBER CORE

These Temperature Maps were computed in a finite-element simulation of thermal conditions on a PWB on which four heat-generating flip chips are mounted. For each of the two cases shown here, the peak temperature mentioned in the text was calculated as an average over all nodal values within the "footprints" of the flip chips.

In one example in the CTE-mismatch analysis, the effective CTE of the region of a carbon-fiber-core where flip chips would be mounted was found to be ≈ 1.0×10^{-5} $(°C)^{-1}$; in contrast, the corresponding CTE of a conventional FR-4 PWB was found to be ≈2.1×10^{-5} $(°C)^{-1}$. Thus, the carbon-fiber core exhibits less CTE mismatch with the chip substrate material — silicon — for which the CTE ranges from 3×10^{-6} to 5×10^{-6} $(°C)^{-1}$. Ultrasonic imaging of carbon-fiber-core FCOB specimens after thermal tests of the specimens revealed that the thermal tests did not result in any detectable increase in the incidence of failures of

flip-chip-mounting solder joints.

This work was done by Eyan Lee and William E. Davis of Applied Material Technologies, Inc., for **Glenn Research Center.**

Inquiries concerning rights for the commercial use of this invention should be addressed to NASA Glenn Research Center, Commercial Technology Office, Attn: Steve Fedor, Mail Stop 4–8, 21000 Brookpark Road, Cleveland, Ohio 44135. Refer to LEW-16890.

Lightweight, Dimensionally Stable Printed-Wiring Boards

In comparison with traditional PWBs, these offer better heat dissipation and CTE matching.

John H. Glenn Research Center, Cleveland, Ohio

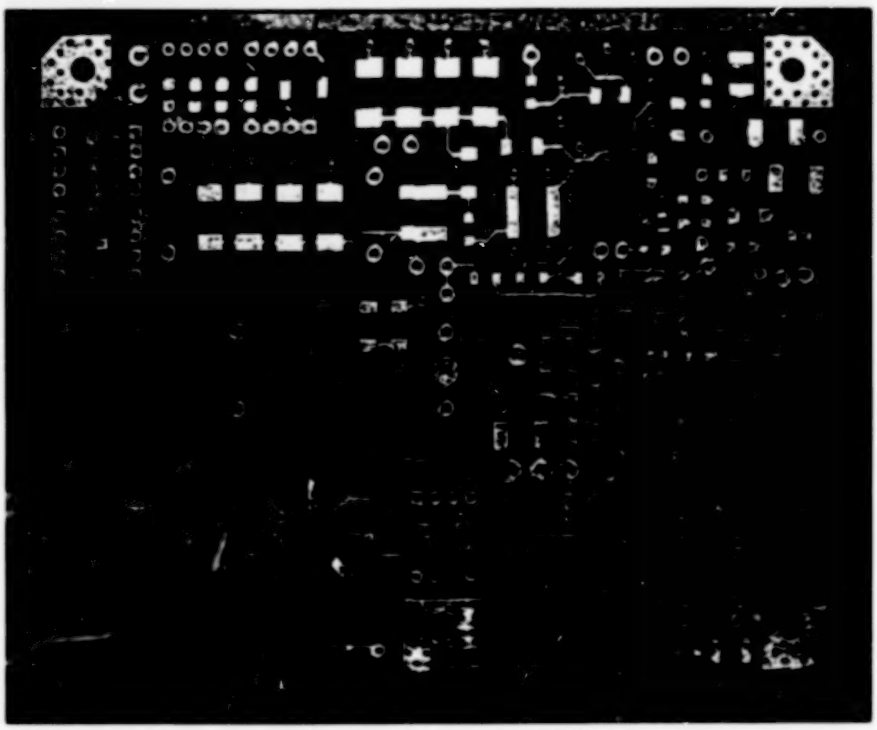

This PWB Contains a Carbon-Cloth Core and a total of eight copper layers. The overall dimensions of the board are approximately 3.25 by 4.25 in. (about 8.3 by 10.8 cm).

Printed-wiring boards (PWBs) that are especially suitable as substrates for highly reliable, lightweight electronic circuits for aircraft and spacecraft have been developed. Like traditional PWBs, these PWBs are laminated composites that include dielectric inner layers plus copper outer layers that can be etched to form signal and power conductors. Going beyond the designs of traditional PWBs, these PWBs include multiple copper layers separated by dielectric (e.g., polyimide) layers, plus inner cores that contain carbon cloth.

These PWBs are intended to accommodate high densities of electronic components and of interconnections among them. The designs of these PWBs can be optimized to satisfy several requirements, including removal of heat generated in electronic components, maximization of stiffness with minimization of weight, and minimization of mismatches between the coefficients of thermal expansion (CTEs) of the PWBs and the components (e.g., leadless chip carriers) mounted on them. Previous solutions to the heat-dissipation and CTE problems have included the use of copper/Invar/copper (CIC) cores. While CIC cores contribute to reduced CTEs and increased thermal conductivities, they also contribute to increases in weights and costs.

Carbon cloth is used in the core layers of the present PWBs because it affords a combination of properties (low CTE, high thermal conductivity, low mass density, and high stiffness) that help to satisfy the requirements mentioned above. [The use of carbon cloth in the core layers of PWBs for this reason is reported in the preceding article, "Mounting Flip Chips on Heat-Dissipating, Matched-CTE Boards" (LEW-16890).] The present carbon-core PWBs offer the advantages, but not the disadvantages, of PWBs with CIC cores; that is, unlike those with CIC cores, these are lightweight and relatively inexpensive. Because of its superior heat-dissipating and CTE characteristics, a PWB of this type (see figure) can accommodate about 40 percent more electronic components than can a traditional PWB.

This work was done by Richard A. Bohner and William E. Davis of Applied Materials and Technologies, Inc., for **Glenn Research Center.**

Inquiries concerning rights for the commercial use of this invention should be addressed to NASA Glenn Research Center, Commercial Technology Office, Attn: Steve Fedor, Mail Stop 4–8, 21000 Brookpark Road, Cleveland, Ohio 44135. Refer to LEW-16648.

Nanoelectronic Devices With Precise Atomic-Scale Structures

Field-effect transistors with nanometer dimensions are under development.

Ames Research Center, Moffett Field, California

Since its invention in 1948, the transistor has revolutionized everyday life. The electronics revolution is based on miniaturization of transistors; smaller transistors are faster, and denser circuitry has more functionality. Transistors in the present generation of integrated-circuit chips have sizes of ≈0.18 μm, and the electronics industry has completed development of 0.13-μm transistors, which will enter production within the next few years. Industry researchers are now working to reduce transistor sizes below 0.1 μm — a thousandth of the width of a human hair. However, studies indicate that the miniaturization of silicon transistors will soon reach its limit.

For further progress in microelectronics, it is necessary to turn to nanotechnology.

Rather than continuing to miniaturize transistors to a point where they become unreliable, nanotechnology offers the new approach of building devices on the atomic scale. One vision for the next generation of miniature electronic circuitry is that of atomic-chain electronics; according to this vision, each device is composed of atoms aligned on top of a substrate surface in a regular pattern. The Atomic Chain Electronics Project (ACEP) — part of a nanotechnology group at Ames Research Center — has been developing the theory for understanding atomic-chain devices, and a patent for atomic-chain electronics has been filed and is now pending.

The use of dopants is critical to the functionality of transistors. Dopants are impurities intentionally added to the semiconducting transistor channel to raise or lower the device switch-on voltage. Typically, a macroscopic transistor (one with a size of the order of 10^{-6} m) contains several thousand dopant atoms that, on the scale of the overall device, appear to be smeared out as a dopant "jelly," as illustrated in the top part of Figure 1. Because of the large number of dopant atoms, the precise location of each dopant atom is not very important to the functioning of the transistor. However, when the size of a transistor is reduced to the range of 10^{-8} to 10^{-7} m, as illustrated in the middle part of Figure 1, the number of dopant atoms is less than about 100, in which case the position of each dopant atom does matter. Current manufacturing techniques do not provide the means to control the locations of the few dopant atoms precisely, and as a result, small variations in functioning occur among transistors. Such variations are fatal when millions or billions of transistors are integrated in a computer chip, because the variations can cascade from one device to the next, eventually giving rise to a malfunction. A solution of this aspect of the miniaturization problem, devised by the ACEP, is to create all the device structures with atomic chains laid out in a regular precise pattern by anchoring atoms to a substrate, as illustrated in the bottom part of Figure 1.

A second critical aspect of the functioning of a transistor is gain: the output of the transistor should be a magnified version of its input. ACEP research has led to the conclusion that in designing atomic-chain transistors to produce gain, one should exploit the field effect, which is the only mechanism verified experimentally so far at the atomic scale. Semiconductors conduct current only when a gate voltage is (is not) applied — field effect. Metals always conduct current. A field-effect transistor uses a semiconductor for the channel and a metal for electrodes, and this is how it achieves large gain. Thus, it is necessary to devise chains with semiconductor and metal properties. First, the ACEP team tackled a simple problem theoretically: If one can arrange silicon atoms along a line floating in air, is this chain semiconducting? The answer is surprising: although bulk or thin-film silicon is semiconducting, an isolated chain of silicon atoms is always metallic. Fortunately, ACEP research also leads to the finding that a magnesium chain is semiconducting, even though bulk magnesium is metallic.

Of course, it is not possible to float atoms in air: it is necessary to place them on top of a substrate. Surface atoms of the substrate attract atoms in the chain and hold them at fixed positions. The surface of a substrate can be made to have atomic-scale corrugations, and these can be used to create a precise pattern for atomic-chain electronics. However, the attractive force between the substrate and chain atoms that are simply placed in the corrugations is too weak to secure atoms reliably. ACEP research has led to the conclusion that a chemical bonding scheme is needed to secure chain atoms reliably, and to the further conclusion that the properties of a chain are strongly influenced by the substrate material and surface orientation when chemical bonding

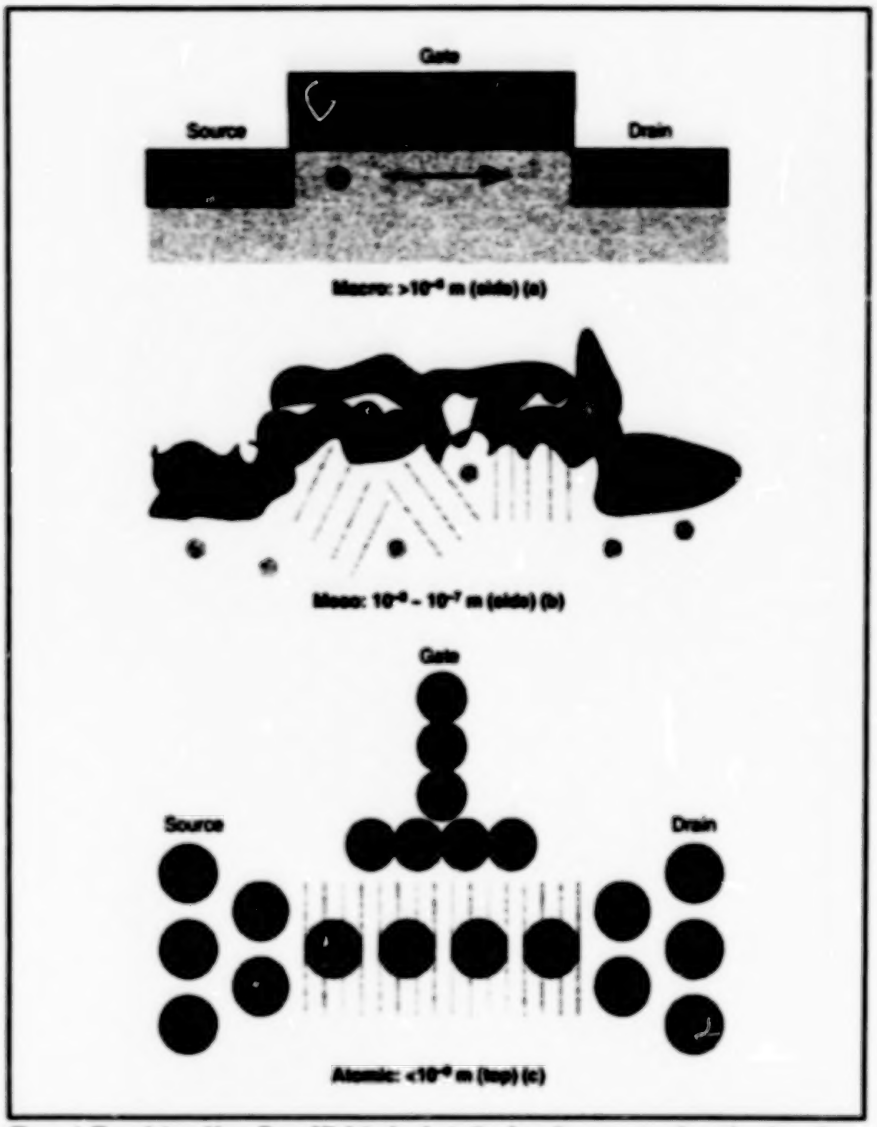

Figure 1. Transistors Have Been Miniaturized, starting from the macroscopic scale, where thousands of dopant atoms can be regarded as being in a smooth distribution that determines the switch-on voltage. At the mesoscopic scale, transistors have different switch-on voltages, depending on precisely where the dopant atoms are located. To prevent such unit-to-unit variations, the next step in miniaturization will not be accomplished by making conventional transistors smaller; instead, transistors with dimensions <1 nm will be made from chains of precisely positioned atoms.

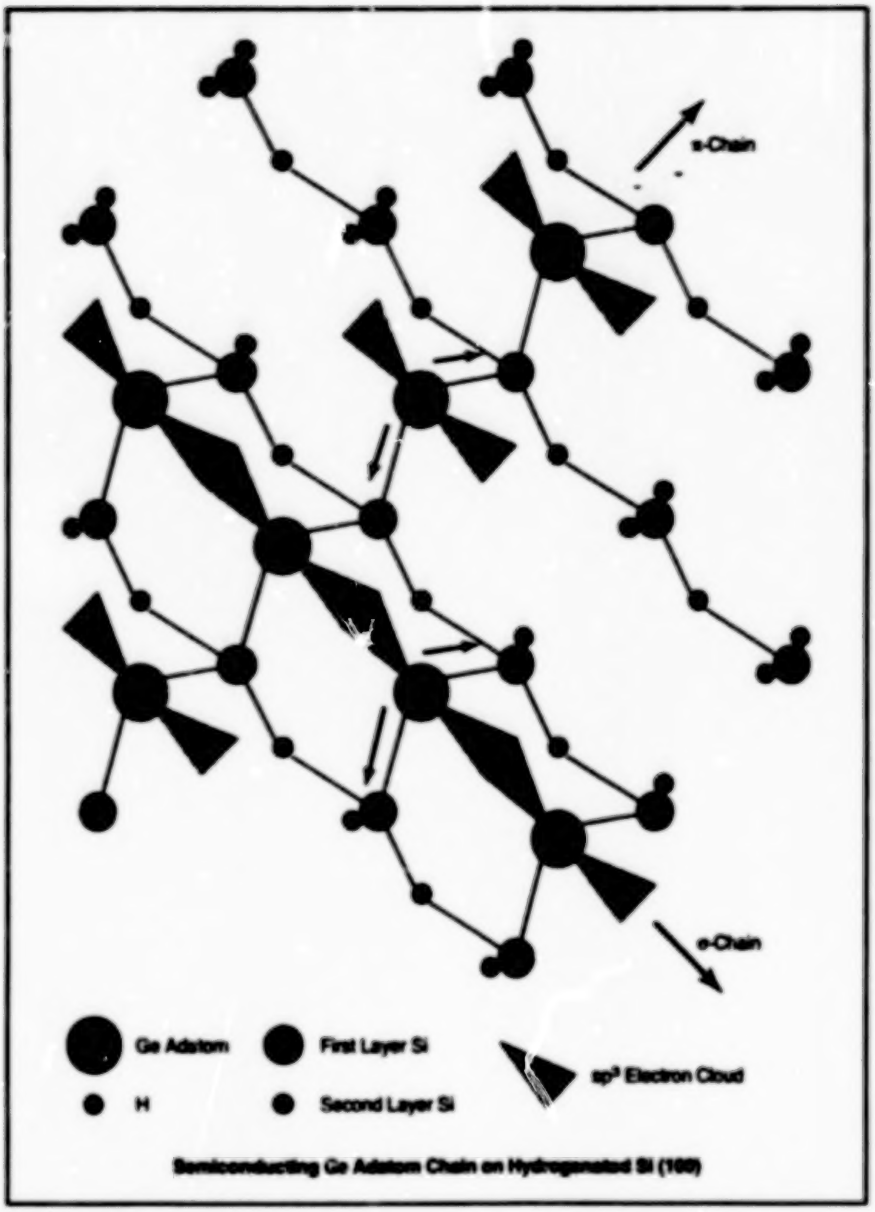

Figure 2. A Semiconducting Chain of Germanium Atoms electrically insulated from other atoms present is formed on top of a (100) silicon substrate, the unused regions of which are hydrogenated.

is used. Indeed, the same atomic chain can be either metallic or semiconducting, depending on the number of chemical bonds between a chain atom and the substrate atoms.

A further concern is that electrons traveling along an atomic chain can detour into the substrate through chemical bonds and possibly leave through a neighboring chain, resulting in the short-circuiting of two atomic chains. Such short circuits are fatal for electronic applications and must be avoided. ACEP research has clarified the conditions under which the substrate surface can be made electrically insulating in a chemical-bonding scheme. Among the findings of this research are that silicon and germanium crystals can be good insulating substrates.

Thus far, the ACEP team has made the first step toward the development of atomic-chain electronic devices. On top of a silicon substrate, it is possible to attach germanium atoms with two chemical bonds each, as shown in Figure 2. The resulting structure is a semiconducting chain on an insulating substrate. Nearby chemical bonds on the substrate are saturated with hydrogen atoms, so that they are electronically inactive. Such a chain can be a component of a field-effect transistor on an atomic scale.

This work was done by Toshishige Yamada of Computer Sciences Corp. for **Ames Research Center.** *Further information is contained in a TSP [see page 1].*

This invention is owned by NASA, and a patent application has been filed. Inquiries concerning nonexclusive or exclusive license for its commercial development should be addressed to the Patent Counsel, Ames Research Center, (650) 604-5104. Refer to ARC-14246.

Books and Reports

PCI Bridge to Instruments and Telecommunication System

A report describes a prototype system interface assembly (SIA) that performs the functions of a compact, radiation-hard application-specific integrated circuit (ASIC) to be built subsequently. The SIA ASIC would be installed in a spacecraft, where it would function as a peripheral-component interface (PCI) with (a) four scientific instruments that generate high-speed serial data streams and (b) either of two spacecraft telecommunication systems — the Small Deep Space Transponder (SDST) or the Space Transponding Modem (STM). Once configured, the serial uplink and downlink channels would conform to the SDST serial interface protocol or the STM modified serial peripheral interface protocol. In the SDST configuration, the downlink could be further configured for Reed-Solomon coding, for turbo coding, for bypass mode, and/or to enable a pseudo-randomizer. The SIA ASIC would operate in conjunction with a bus controller/remote terminal/monitor ASIC (United Technologies BCRTM or equivalent) to provide the control and status interfaces to the telecommunication systems and/or other systems that conform to MIL-STD-1553 devices. The ASIC would control, and would serve as an interface to, memory circuitry configurable by the user as external first-in/first-out buffers for each of the telecommunication and instrument interfaces.

This work was done by Anwar Akhtar, Martin Lee, John Gilbert, Alfred Khashaki, Carl Steiner, Donald Johnson, Dwight Geer, Julianne Romero, Kazo Ishikawa, Kenneth Crabtree, and Leonard Day of Caltech for **NASA's Jet Propulsion Laboratory.** *To obtain a copy of the report, "PCI Bridge to Telecom and Four Instrument Interfaces," see TSP's [page 1].*

NPO-30278

Electronic Systems

Hardware, Techniques, and Processes

13 Fiber-Optic Phase-Locked Loop Sensitive to Local Strain Only
14 Parallel-Processing High-Rate Digital Demodulator ASIC
15 TAXI Direct-to-Disk Interface Demultiplexes Proprietarily Formatted Data
16 Reusable Software for Autonomous Diagnosis of Complex Systems

12

BLANK PAGE

Fiber-Optic Phase-Locked Loop Sensitive to Local Strain Only

Optical fibers are made insensitive to strain except over a short sensory length.

Langley Research Center, Hampton, Virginia

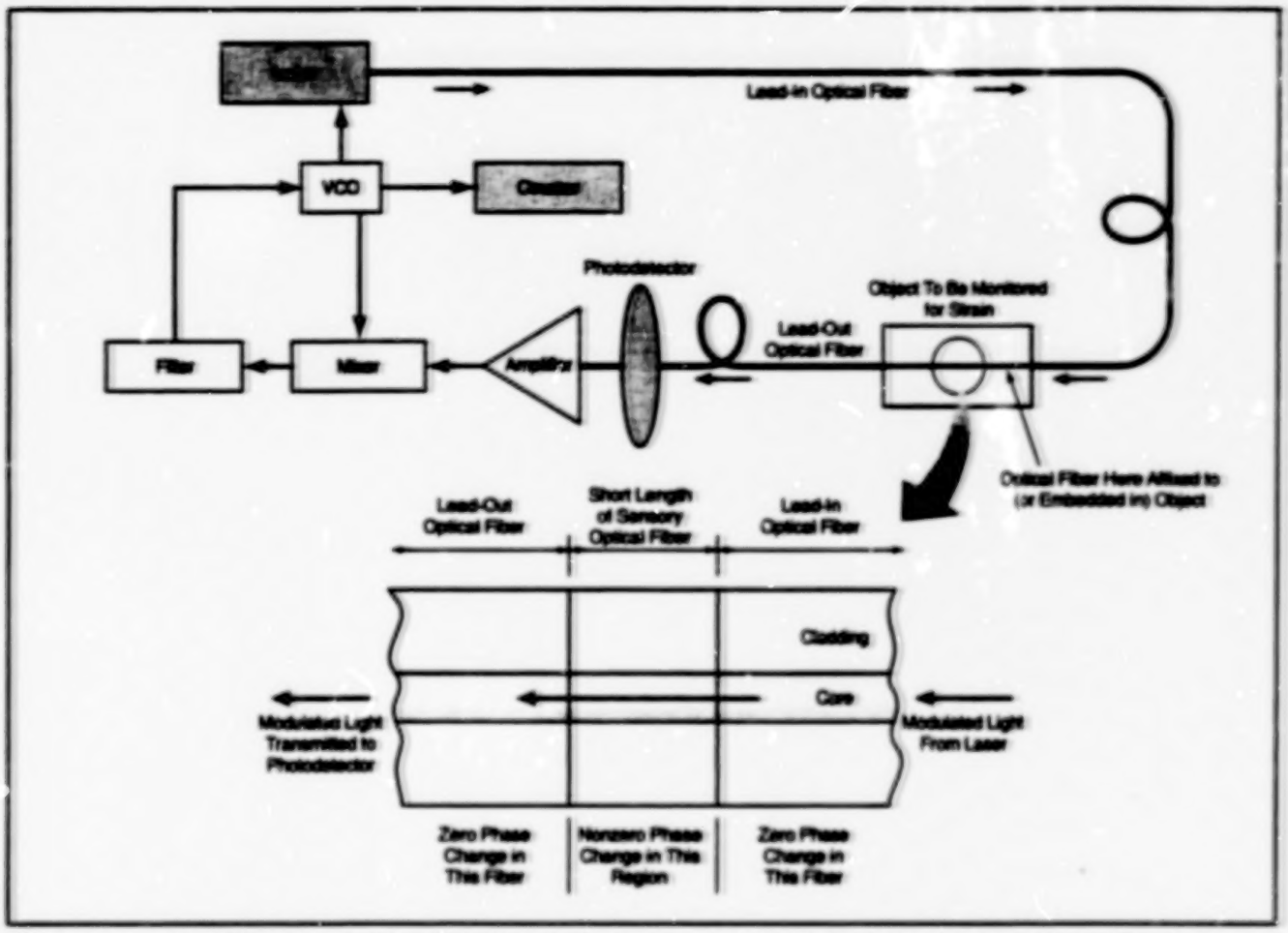

The Frequency of the VCO in this optical phase-locked loop changes in response to strain in the short sensory length of optical fiber. Strain in the lead-in and lead-out lengths of fiber does not cause the frequency to change.

The figure schematically depicts an apparatus for measuring strain at only one designated location on a structure. The apparatus is a fiber-optic phase-locked loop, wherein strain in a multimode optical fiber gives rise to a change in the phase of modulation of a laser beam that propagates along the fiber. The optical phase-locked loop makes it possible to perform sensing by use of a multimode optical fiber (in contradistinction to a single- or few-mode fiber as in some other fiber-optic sensor systems). Unlike in other fiber-optic-based sensor systems, the phase change in this system does not occur in response to strain integrated along the entire fiber-optic path. Instead, this system includes lead-in and lead-out strain-insensitive lengths of optical fiber connected to a short strain-sensitive length of optical fiber that is affixed to the structure at the desired measurement location. Strain in the short sensory length produces a phase change, but strain in the lead-in and lead-out portions does not.

The output of a voltage-controlled oscillator (VCO) is used to modulate the laser light and to supply a reference signal to a double balanced mixer. After traveling along the strain-insensitive and strain-sensitive lengths of optical fiber, the modulated laser signal impinges on a photodetector, the output of which is amplified and mixed with the reference signal. A filter removes the radio-frequency component of the mixer output, passing only the DC or low-frequency component, which component constitutes a DC error voltage. The phases of the fiber-optic-propagated and reference signals are maintained at quadrature by feedback of the DC error voltage to the VCO. A change (caused by strain) in the phase of the modulation manifests itself as an error voltage and, by virtue of the feedback, is compensated by a change in the modulation frequency. The frequency is monitored by a counter.

A multimode optical fiber can be made more or less sensitive to strain through selection of the fiber core and cladding materials. Assuming that the fiber can be approximated as weakly guiding (meaning, essentially, that the index of refraction of the core exceeds that of the cladding by an amount $\ll 1$), it can be shown that the condition for complete insensitivity to strain (zero phase shift in response to strain) is given by

$$n_{core} = (2/P_{eff})^{1/2},$$

where n_{core} is the index of refraction,

$$P_{eff} = [P_{12} - \nu_f(P_{11} - P_{12})]/2,$$

ν_f is the Poisson's ratio of the fiber, and P_{11} and P_{12} are the strain-optic coefficients of the fiber.

The insertion of appropriate parameters in these equations leads to the conclusion that a strain-insensitive optical fiber is one in which the core has a very high index of refraction (4.5 is an approx-

imate representative value). Germanium is one example of a material suitable for a multimode optical fiber with a very high index of refraction.

This work was done by Claudio O. Egalon and Robert S. Rogowski of **Langley Research Center.** *Further information is contained in a TSP [see page 1].*

This invention has been patented by NASA (U.S. Patent No. 5,780,844). Inquiries concerning nonexclusive or exclusive license for its commercial development should be addressed to Rheal Turcotte, Technology Commercialization Program Office, NASA Langley Research Center at (757) 864-8881 or e-mail at r.p.turcotte@larc.nasa.gov. Refer to LAR-15159.

Parallel-Processing High-Rate Digital Demodulator ASIC

CMOS circuitry can be used instead of more expensive analog circuitry or GaAs-based kind.

NASA's Jet Propulsion Laboratory, Pasadena, California

An all-digital demodulator has been developed for receiving radio signals with multigigahertz carrier frequencies phase-modulated with digital data signals at bit rates of hundreds of millions of bits per second. The phase modulation could be either binary phase-shift keying (BPSK) or quadrature phase-shift keying (QPSK), including QPSK employing bandwidth efficient pulse-shaping methods. The demodulator has been implemented in complementary metal oxide semiconductor (CMOS) application-specific integrated circuit (ASIC) configured to utilize algorithms that process signal data in multiple parallel streams.

The advantages of all-digital processing over traditional analog processing include greatly increased flexibility and reliability with reduced reproduction costs. Serial digital signal processing would entail processing rates so high as to necessitate the use of non-CMOS (e.g., GaAs-based) circuitry, which costs more and is more power-hungry, relative to CMOS. What makes it possible to implement the present ASIC in CMOS is the parallel-processing scheme, in which the number of parallel data streams is made large enough that the data rate in each stream is low enough to be within the capability of CMOS circuitry.

The present all-digital demodulator is characterized by an advanced parallel receiver (APRX) architecture (see figure), which replaces the receiver functions of the parallel receiver (PRX) architecture reported in "Parallel Digital Demodulators Using Multirate Filter Banks" (NPO-19620), *NASA Tech Briefs*, Vol. 20, No. 10 (October 1996), page 65. The APRX architecture is essentially one of time-varying frequency-domain detection filtering and symbol-timing correction.

Upstream of this demodulator, the received analog signal is converted to an intermediate frequency (IF) suitable for analog-to-digital (A/D) conversion, band-pass filtered, then digitized at a rate of 4 samples per symbol. The band-pass filtering rejects some noise and prevents the aliasing that would otherwise occur after A/D conversion. The digital signal is split into 32 parallel paths, decimated by 16 on each path, and digitally mixed on each path with a replica of the sampled IF carrier signal. The discrete Fourier transform (DFT) of the resulting 32 data points is then taken, via a specialized fast Fourier transform (SFFT), and multiplied by the one element of a bank of frequency-domain-matched filters. The correct matched filter is chosen by the closed-loop symbol timing recovery algorithm (see figure).

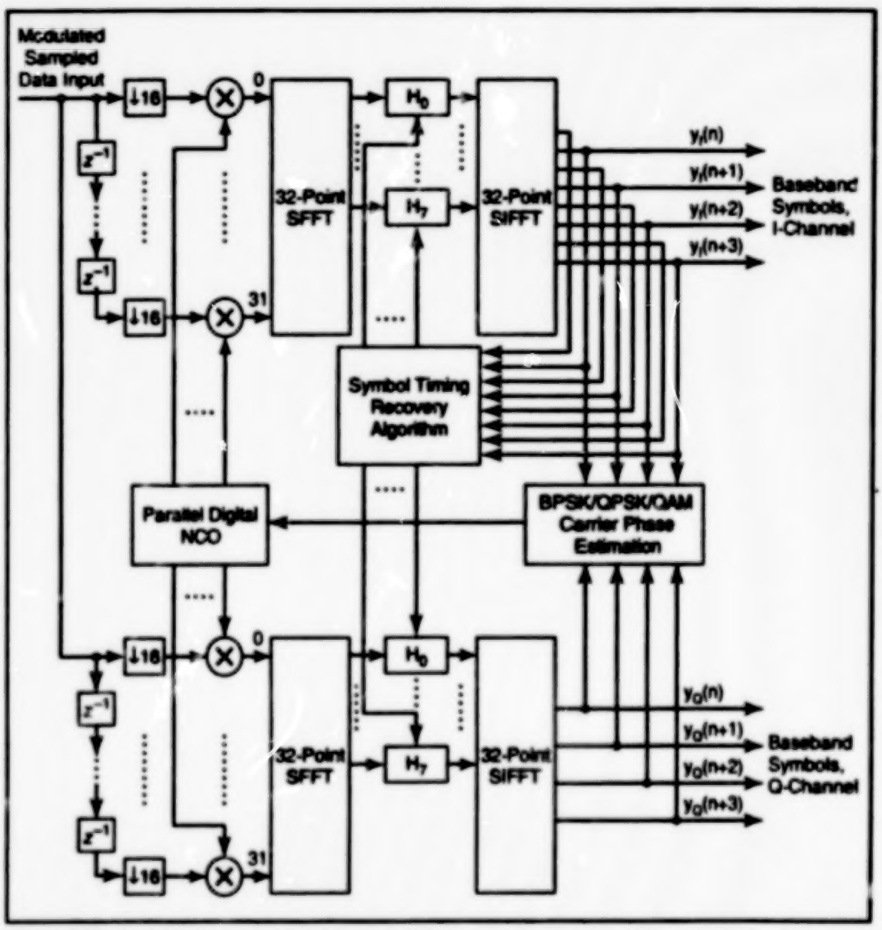

The APRX Architecture provides for most digital signal processing to be done in the frequency domain. Here, "z^{-1}" denotes a digital sample delay, "↓16" signifies decimation by a factor of 16, and H_i denotes a complex time-varying matched/detection filter bank that also performs the functions of low-pass digital filter and symbol timing recovery.

To suppress the double-frequency terms generated in mixing to baseband, low-pass filtering is performed, zeroing out the middle 16 components (which correspond to the high-frequency terms) in the frequency domain. Then the inverse discrete Fourier transform (IDFT) is computed, via the specialized inverse fast Fourier transform (SIFFT), and the middle 16 parallel outputs (which are unaliased and correspond to 4 symbol periods) are used for detection, tracking, and other purposes.

The foregoing process is repeated once every 16 cycles of the A/D-converter clock. The 16 points in the SIFFT output are 16 samples of a convolution of the input

sequence with the matched-filter impulse-response function. Among these 16 samples are 4 baseband symbols that correspond to the peak signal-to-noise-ratio outputs of the matched filter.

Theoretical analysis, computational simulations, laboratory tests, and live satellite downlinks have shown that the error-rate performance of the APRX demodulator can be expected to be equivalent, and in some cases superior, to that of a conventional serial-processing digital receiver. In comparison with the PRX architecture, the APRX architecture can be implemented with significantly reduced complexity. In comparison with traditional serial digital receivers, the APRX demodulator ASIC can process much higher data rates. The next generation implementation of the APRX ASIC is currently being developed to process higher order modulations and data rates in excess of 2 billion bits per second.

This work was done by Parminder Ghuman, Scott Hoy, and Gerald Grabowsky of Goddard Space Flight Center and Andrew Gray and Meera Srinivasan of Caltech for **NASA's Jet Propulsion Laboratory.** *Further information is contained in a TSP [see page 1].*
NPO-21230

TAXI Direct-to-Disk Interface Demultiplexes Proprietarily Formatted Data

Data can be stored in channel files in a PC in real time.

Stennis Space Center, Mississippi

The TAXI Direct-to-Disk interface is a special-purpose interface circuit for demultiplexing of data from a Racal Storeplex (or equivalent) multichannel recorder onto one or more hard disks that reside in, and/or are controlled by, a personal computer (PC). [The name "TAXI" as used here is derived from the acronym TAXI, which signifies transparent asynchronous transceiver interface.] The TAXI Direct-to-Disk interface was developed for original use in capturing data from instrumentation on a test stand in a NASA rocket-testing facility. The control, data-recording, and data-postprocessing equipment of the facility are located in a control room at a safe distance from the test stand. Heretofore, the transfer of data from the instrumentation to the postprocessing equipment has entailed post-test downloading via software, requiring many hours to days of post-test reduction before the data could be viewed in a channelized format. The installation of the TAXI Direct-to-Disk interface, in conjunction with other modifications, causes the transfer of data to take place in real time, so that the data are immediately available for review during or after the test.

The instrumentation is connected to the input terminals of the signal-processing unit of multichannel recorder by standard coaxial cables. The coaxial output of the signal-processing unit is converted to fiber-optic output by means of a commercial coaxial-cable/fiber-optic converter (that is, a fiber-optic transceiver) designed specifically for this application. The fiber-optic link carries the data signals to an identical fiber-optic transceiver in the control room. On the way to the TAXI Direct-to-Disk interface that is the focus of this article, the data signals are processed through a companion special-purpose circuit denoted by the similar name "parallel TAXI interface" (see figure).

The TAXI Direct-to-Disk interface is implemented by means of field-programmable gate arrays (FPGAs), memory chips, and other integrated circuits on a printed-circuit board that conforms to the peripheral component interface (PCI) standard and is denoted the TAXI-100 card. The TAXI-100 card performs real-time demultiplexing of the data signals from the parallel TAXI Direct-to-Disk interface to individual channel files within the host PC. The data are provided in a layered interface that consists of the TAXI physical layer with the Racal proprietary data format contained in the application layer. The application layer is stripped off by the parallel TAXI Direct-to-Disk interface. Parallel clock and data signals containing the Racal proprietary data format are received by the TAXI-100 card in the parallel format and demultiplexed, according to formats extracted from within the data, into channel buffers in the form of first-in/first-out (FIFO) memory chips. Other proprietary programmable logic chips provide for the management and buffering of the channel blocks until they are presented to the host PC across a PCI bus inter-

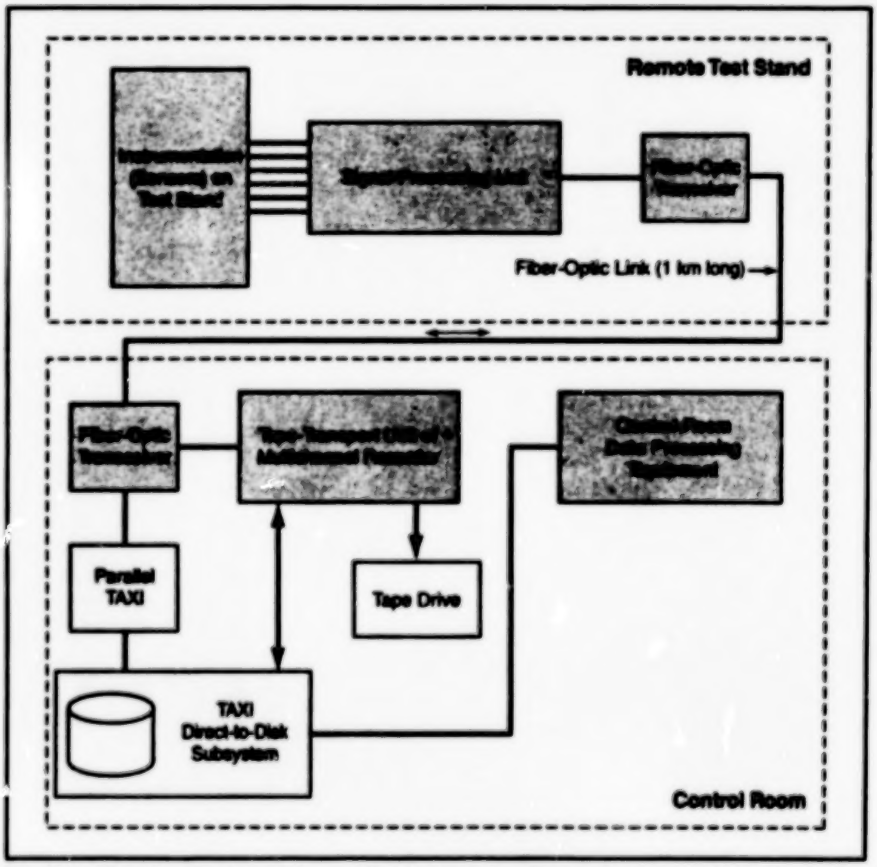

The Data-Flow Architecture of the modified test-data-handling system of a rocket-testing facility includes the parallel TAXI Direct-to-Disk interface and the TAXI-100 Direct-to-Disk interface solution.

face. Real-time software drivers running under the Microsoft NT 4.0 operating system provide for real-time handling of interrupts and buffering onto small computer systems interface (SCSI) disks in individual channel files. A host graphical user interface enables the user to select recorder channels.

This work was done by Bruce G. Newman of Integrated Systems Consultants and Steven F. Ahlport of Pacific Custom Systems, Inc., for **Stennis Space Center.**

In accordance with Public Law 96-517, the contractor has elected to retain title to this invention. Inquiries concerning rights for its commercial use should be addressed to

Integrated Systems Consultants
1282 Shasta Ave.
Suite 1
San Jose, CA 95126

Refer to SSC-00141, volume and number of this NASA Tech Briefs *issue, and the page number.*

Reusable Software for Autonomous Diagnosis of Complex Systems

Software incorporates advances in several data analysis disciplines to enable autonomous self-monitoring.

NASA's Jet Propulsion Laboratory, Pasadena, California

A software system designed to provide a purely signal-based diagnosis of virtually any time-varying system has been developed. This software is part of an overall concept called "Beacon-based Exception Analysis for Multimissions," or BEAM. This concept provides for real-time autonomous diagnostics and prognostics of virtually any complex system (e.g., intelligent spacecraft or advanced aircraft) by use of software executed on an embedded computer.

BEAM provides for the onboard identification and isolation of anomalous conditions, making it unnecessary to telemeter large quantities of raw data for analysis on the ground. BEAM thereby reduces operator or pilot workload by isolating all anomalies that could affect safety, navigation, or performance. BEAM was conceived as an incrementable autonomy technology, capable of operating with no human intervention but also supplying condensed information to aid human operating decisions. Thus, the system is useful at both extremes, viz, total autonomy and complete operator control, and at every level in between.

This particular component of BEAM, called the System Invariant Estimator (SIE), uses strictly signal-processing methods and is therefore highly reusable. Many approaches to the problem of self-diagnosis exist, such as model-based and neural network solutions. However, in many cases these approaches require significant investment in modeling and training, perform poorly beyond the model or training envelopes, and perform poorly in the presence of data uncertainty. Because of BEAM's underlying architectural differences from these approaches, a priori modeling is useful but not necessary, the training process is relatively simple and is incrementable, and the system is capable of correctly isolating anomalies well outside the training envelope.

The SIE provides a standard method for real-time fusion and analysis of all time-varying system observables, including sensor data as well as derived quantities and certain quantifiable software indications. These data sources can be from similar sensors or from radically varying types. The intermediate information products of the SIE retain considerable physical meaning, which allows complete traceability of the diagnostic state and reconstruction of the BEAM conclusions. The SIE provides detection capability, in both space (signal localization) and time, for both sudden and gradual changes in any system. The approach is readily scalable to systems of higher complexity and is resistant to the usual problem of combinatoric explosion as system size increases.

The SIE functions by considering the cobehavior of time-varying quantities, in particular their dynamics, as sensed from an operating system. Suitable sensors are widely used and typically include so-called performance sensors, i.e., temperatures, pressures, and the like. Certain repeatable relationships between physical quantities, and, hence, sensor values, exist in the system as dictated by the physics of its operation. These relationships are repeatable and relatively insensitive to changes in the environment or normal fluctuations.

The SIE constructs a single quantitative object to capture this cobehavior across the entire system or subsystem. This object reflects both known relationships, such as voltage/current relationships that are easily modeled, and unknown relationships, such as thermal transmission through system structure that is not well understood. The object is studied with respect to stability, for the purpose of detecting instantaneous changes or mode switches, and its long-term convergence, which reveals the presence of incipient faults, degradations, or minor and local shifts away from desired performance. This allows us to consider the entire space of faults, including those for which modal information or even data is not available.

The SIE is a computationally efficient calculation grounded entirely in signal theory. It is trained using raw sensor data during known nominal operation, i.e., "supervised" training. This data would ideally cover all nominal modes. However, should this be impossible to obtain, or if only approximate data is available, the SIE can be executed in a learning mode. This is possible because the SIE is capable of capturing "novel" data as part of its anomaly detection, and should this data prove to be acceptable upon review, it can be incrementally added to the SIE training. The only needed human effort is providence of nominal data; all other training and detection is completely autonomous.

The SIE can accept time-correlated input data from relatively large sources. Its specific outputs are the presence of off-nominal behavior or degradation, the signals implicated in the fault, and a predictive assessment of loss of functionality. It also identifies specific pair-wise resonances contributing to the fault (critical for assessing control-loop-induced failures), renormalization functions to quantify intramodal stability and degradation, and capture of off-nominal flight data to allow adaptation to new modes or specific hardware.

Unlike similar neural network approaches, each information product of BEAM has an implicit physical meaning. Where uncertainties about the diagnosis exist, each step towards constructing the ISE (information space estimate) and its analysis can be performed individually. This provides operators the maximum utility in managing system information. This property also allows BEAM to optimally summarize fault information for downlink.

The present software has been applied to a broad variety of systems and has demonstrated enormous potential in improving system operability while reducing operator workload. Systems previously studied have spanned from 6 to 1,600 observables, and at various data rates from 0.016 Hz to 10 kHz.

This work was done by Sandeep Gulati and Ryan Mackey of Caltech for **NASA's Jet**

Propulsion Laboratory. *Further information is contained in a TSP [see page 1].*

In accordance with Public Law 96-517, the contractor has elected to retain title to this invention. Inquiries concerning rights for its commercial use should be addressed to

Technology Reporting Office
JPL
Mail Stop 249-103
4800 Oak Grove Drive
Pasadena, CA 91109
(818) 354-2240

Refer to NPO-20803, volume and number of this NASA Tech Briefs issue, and the page number.

BLANK PAGE

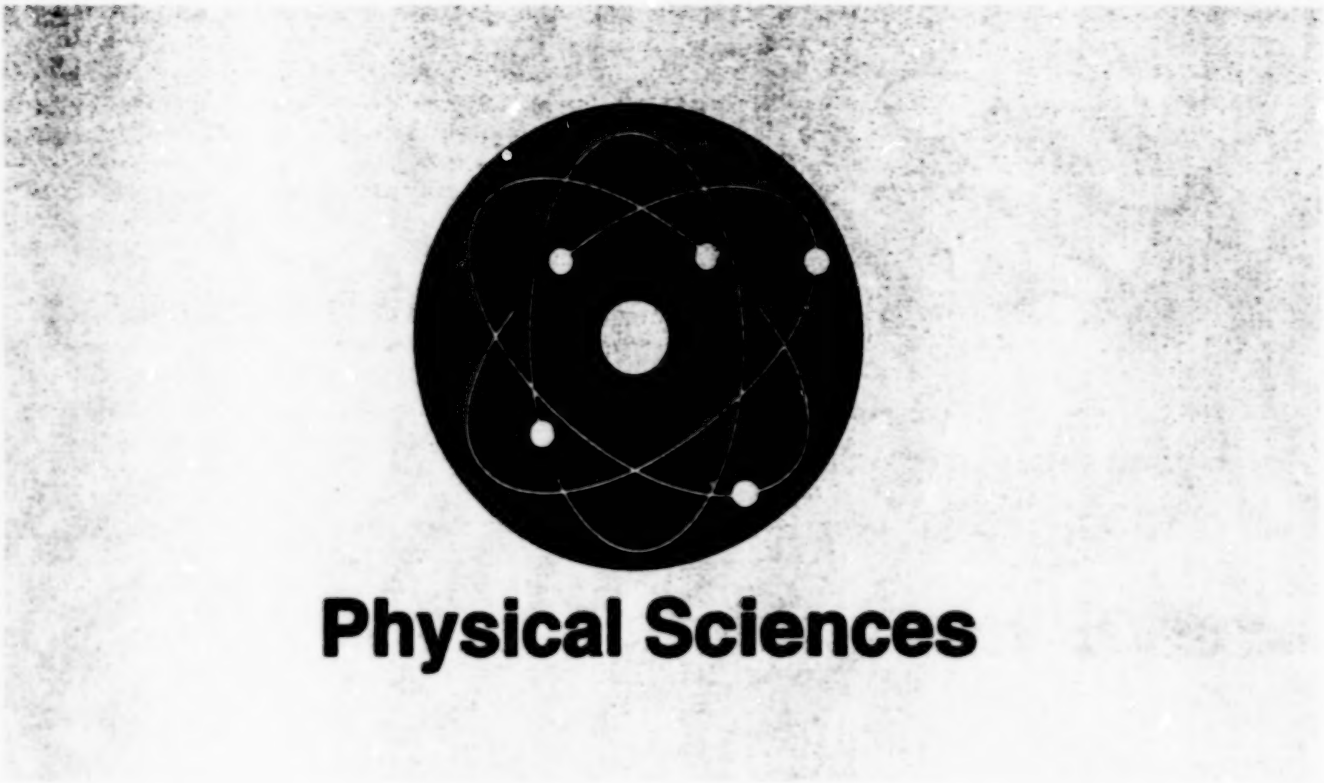

Physical Sciences

Hardware, Techniques, and Processes

21 Light Recycling and Color Scrolling for Brighter Displays
22 Testing Grazing-Incidence Mirrors at Nearly Normal Incidence
24 Portable Instrument Detects Very Dilute Airborne Organics
25 Electrochemical Systems Generate Ozone and Ozonated Water
26 Liquid-Crystal Phase-Shifting Shearing Interferometer
27 Phase-Retrieval Camera for Optical Testing
28 Solar Simulator for a Portable Solar-Absorptance Instrument

Books and Reports

28 Quantum Mechanics of Harmonic Oscillator in External Fields
29 Effect of Gravitation on Noninteracting Trapped Fermions

BLANK PAGE

Light Recycling and Color Scrolling for Brighter Displays

Two efficiency-enhancing techniques would be combined.

NASA's Jet Propulsion Laboratory, Pasadena, California

The efficiencies and thus the brightnesses of flat-panel projectors based on liquid-crystal devices (LCDs) and digital mirror devices (DMDs) would be increased by the combination of a color-scrolling technique and a light-recycling technique, according to a proposal. These techniques were originally proposed separately for the purpose of increasing the efficiencies of LCD-based display devices.

The scrolling-color technique was reported previously in "Using Surface-Plasmon Filters To Generate Scrolling Colors" (NPO-20110), *NASA Tech Briefs*, Vol. 23, No. 2 (February 1999), page 14a. To recapitulate: by use of prisms and surface-plasmon tunable filters, white light from a lamp or other illumination source would be converted into a pattern of scrolling primary colors. The advantage of this scheme is that both polarization components and all colors would be utilized, whereas in prior schemes, most of the light power is wasted through color and/or polarization filtering.

The light-recycling technique was reported in "Low-Absorption Color Filters for Flat-Panel Display Devices" (NPO-20435), *NASA Tech Briefs*, Vol. 23, No. 12 (December 1999), page 34. In this technique, one would replace traditional dye filters with surface-plasmon or interference filters, which are more reflective than absorptive. In addition, the filter and illumination optics would be arranged so that much of the light in all colors and both polarizations reflected from the filters would be sent back through the light-source optics to be reused as illumination.

The present proposal calls for, among other things, a white light source equipped with a reflector and a color-recycling and -scrolling panel (CRSP), as shown schematically in the upper part of Figure 1. The CRSP would contain an array of voltage-tunable or voltage-switchable filters, each of which would transmit one primary color (red (R), green (G), or blue (B), depending on the applied voltage) and reflect the other two primary colors. The reflected light would be bounced back and forth between the CRSP the light-source reflector until light of each color impinged on its proper color filter. Thus, light in the three colors would be redistributed as needed and relatively little would be lost.

At the first phase of a three-phase operating cycle, the color-filter array could be energized to a color pattern as RGB . . . , for example. In the next phase, the color pattern could be changed to BRG . . . . In the third phase, the color pattern could be changed again to GBR . . . . The net result is that recycling and scrolling of colors would occur in combination. The number of color filters need not match the number of pixels in the display panel to be illuminated; the only requirement on the number of filters is that it be an integer multiple of 3.

The voltage-tunable or voltage-switchable color filters could be surface-plasmon tunable filters (see "Voltage-Tunable Surface-Plasmon Band-Pass Optical Filters" (NPO-19988), *NASA Tech Briefs*, Vol. 22, No. 8 (August 1998), page 18a). Alternatively, they could be assemblies of interference or thin-metal film filters, high-index-of-refraction prisms, and total-internal-reflection switches (see "Digitally Tunable Color Filters and Beam Scanners" (NPO-20240), *NASA Tech Briefs*, Vol. 23, No. 9 (September 1999), page 65) that would include layers of an electro-optical material between prisms, as

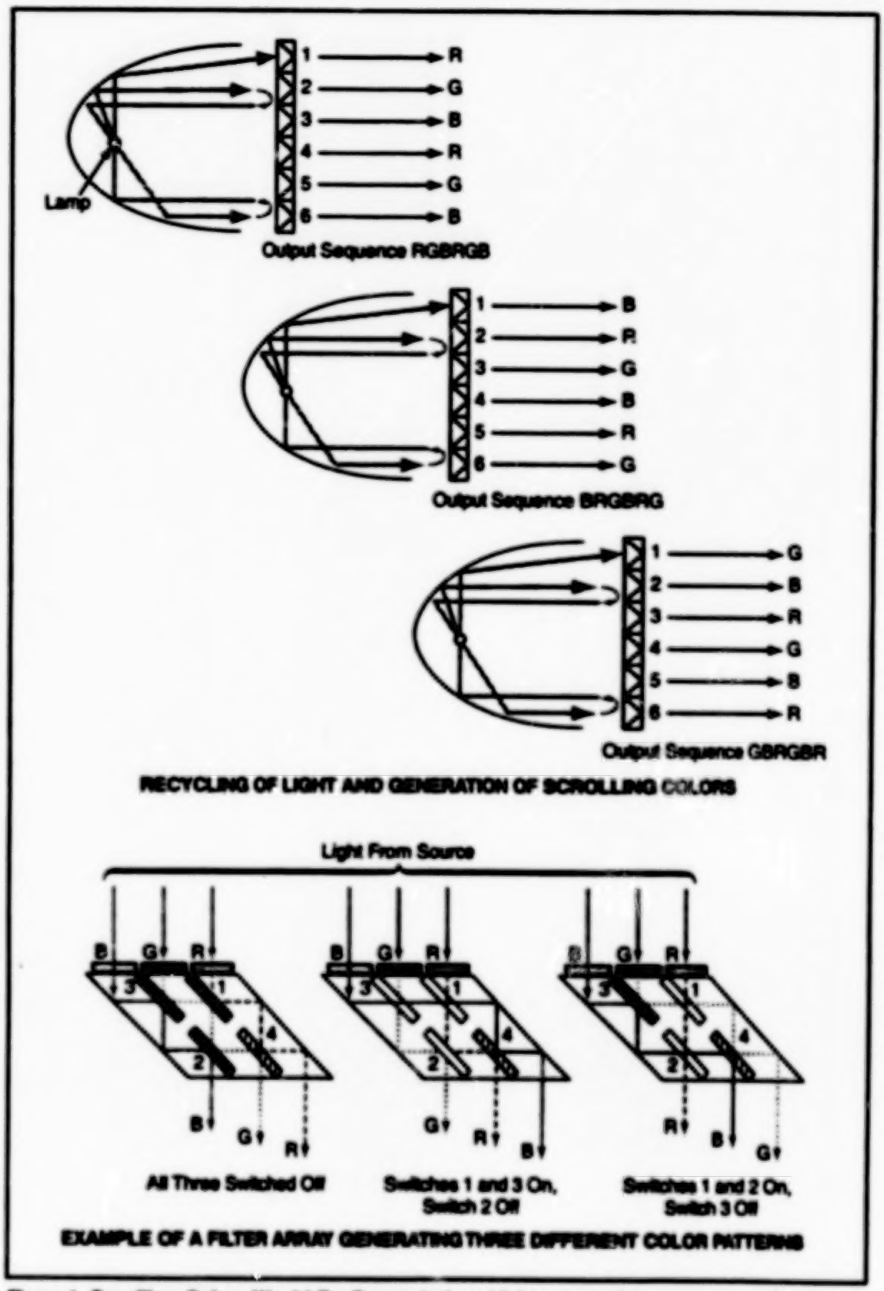

Figure 1. Scrolling Colors Would Be Generated, and light not used to generate scrolling colors on the first pass would be recycled and so used on subsequent passes.

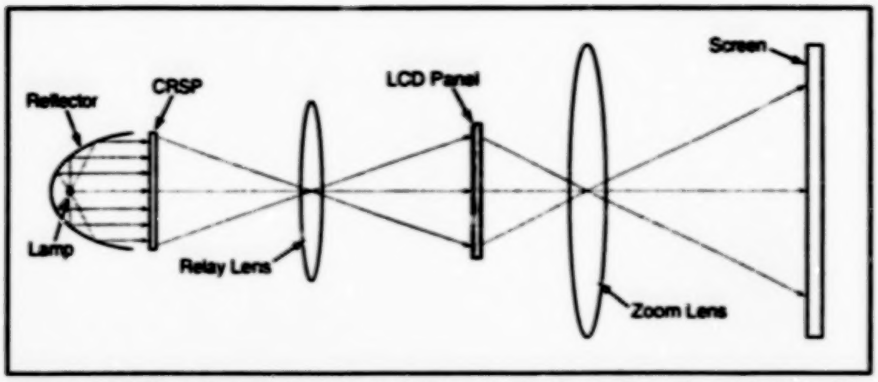

Figure 2. A Flat-Panel Projector based on an LCD would utilize the scrolling-color and light-recycling techniques for maximum light-utilization efficiency.

shown in the lower part of Figure 1. In the absence of applied voltage, the electro-optical layer in each switch would have a low index of refraction, so that total internal reflection would occur at the prism/switch interfaces. The application of a sufficient voltage to the switch would increase the index of refraction of the electro-optical layer sufficiently to allow light to pass through. By appropriate switching in this manner, one can cause light of the various colors to travel along various paths in the prisms to obtain various output color patterns.

Figure 2 presents an example of an LCD-based display system that would include a CRSP. The image of the CRSP would be projected into a monocolor LCD panel by a relay lens. A zoom lens would project an image of the LCD onto a screen. It would be necessary to use an electronic driver that would synchronize the scrolling of colors and the modulation of light by the LCD. Similar geometry can be applied to DMDs.

This work was done by Yu Wang of Caltech for **NASA's Jet Propulsion Laboratory**. *Further information is contained in a TSP [see page 1].*

In accordance with Public Law 96-517, the contractor has elected to retain title to this invention. Inquiries concerning rights for its commercial use should be addressed to

Intellectual Property group
JPL
Mail Stop 202-233
4800 Oak Grove Drive
Pasadena, CA 91109
(818) 354-2240

Refer to NPO-21052, volume and number of this NASA Tech Briefs *issue, and the page number.*

Testing Grazing-Incidence Mirrors at Nearly Normal Incidence

This system enables adequate testing in visible light, without need for a vacuum system.

Goddard Space Flight Center, Greenbelt, Maryland

An optical system that utilizes visible light at nearly perpendicular incidence has been invented for use in testing the surface figures of nominally axisymmetric (paraboloidal, ellipsoidal, or conical) mirrors designed to function at grazing incidence. Such mirrors can be used as the focusing optical elements of x-ray telescopes and x-ray cameras. As explained below, the present system offers advantages over prior systems used to test such mirrors.

It is possible to test a grazing-incidence x-ray mirror by use of visible light at grazing incidence, but diffraction at visible wavelengths limits the achievable angular resolution to the order of one arc minute, whereas a resolution of 15 arc seconds or finer is typically needed for proper diagnosis of the surface figure. It is possible to test such a mirror at finer resolution by use of x rays at grazing incidence in the intended operational configuration, but testing in this way is of limited diagnostic value. Moreover, to prevent excessive absorption of x rays, x-ray testing must be performed in a vacuum chamber: this makes it difficult and time-consuming to manipulate the mirror and test equipment, thereby making testing expensive. The present system utilizes nearly perpendicular incidence to overcome the deleterious effect of diffraction, making it possible to

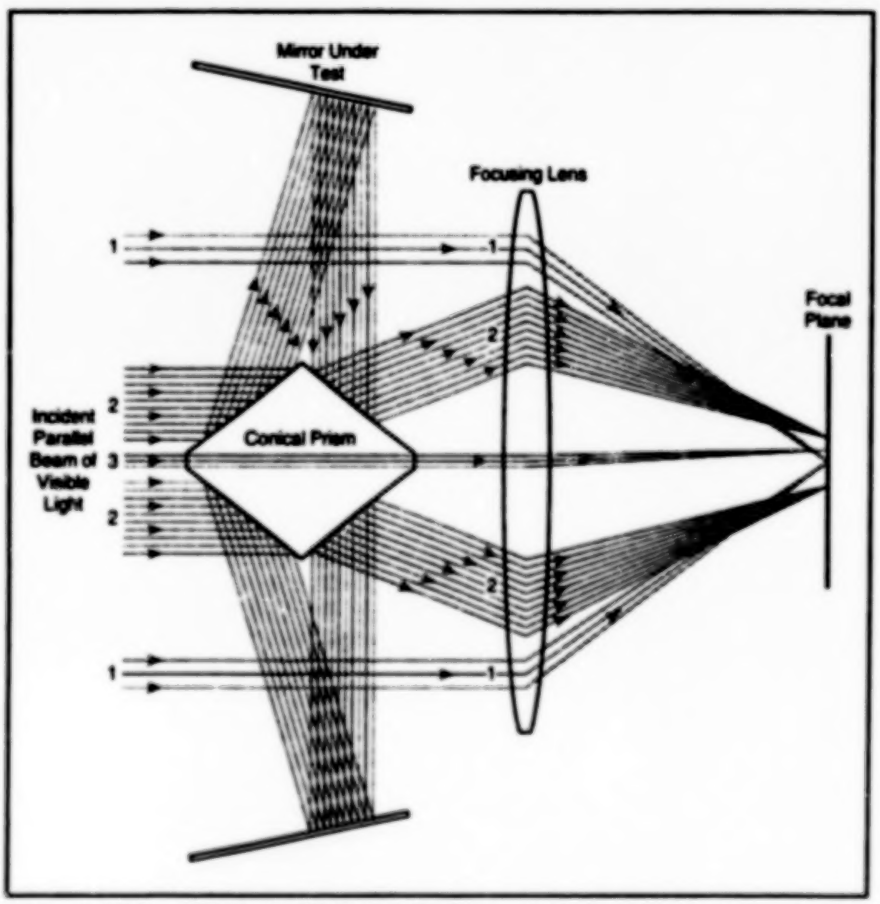

Figure 1. A Prism With Conical Reflective Surfaces, suitably dimensioned and aligned, acts in conjunction with a focusing lens and with the mirror under test to form images indicative of the surface figure of the mirror and the alignment of the mirror with respect to the prism.

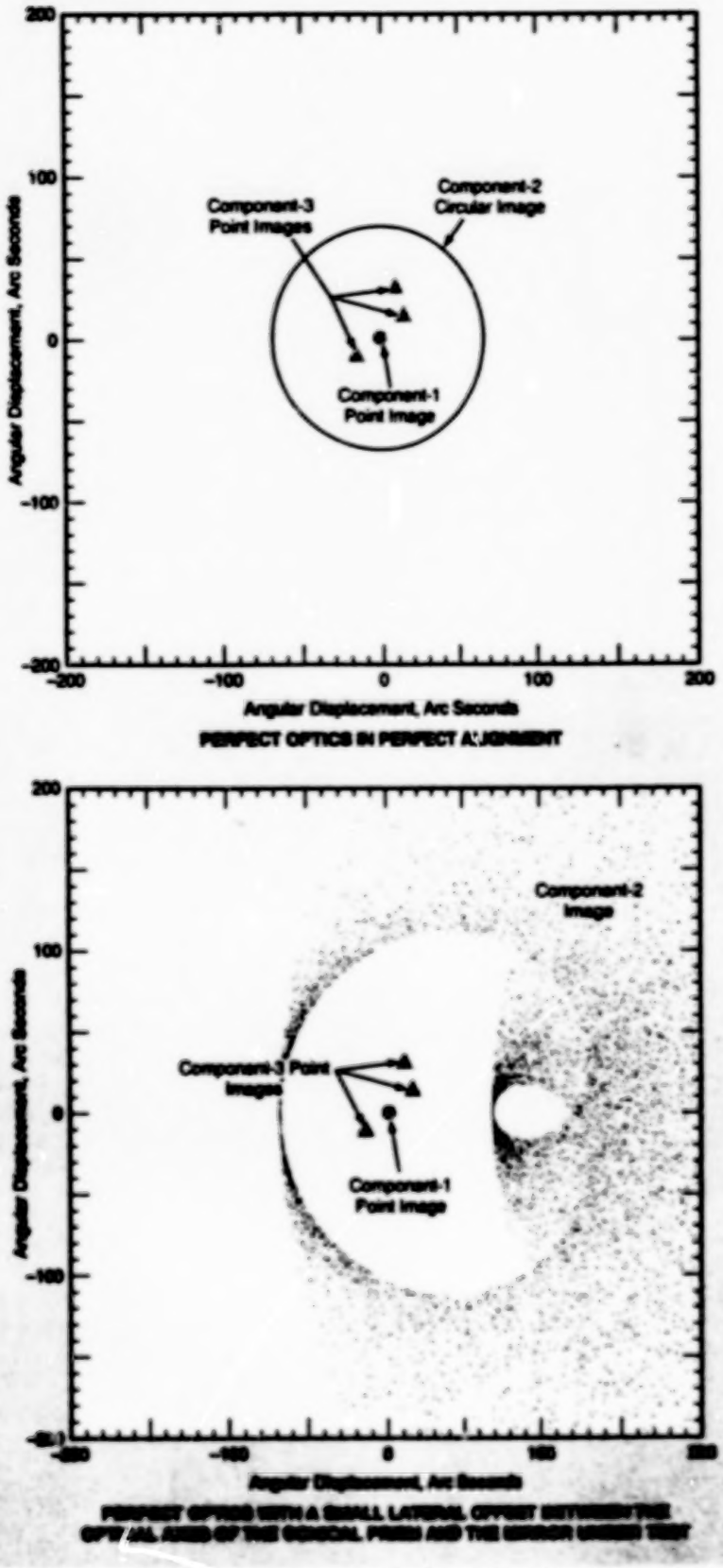

Figure 2. These Images Are Typical of a system like that of Figure 1 in which perfect optics are tested in perfect and imperfect alignment, respectively.

obtain angular resolution of a few arc seconds with visible light and, hence, without need for a vacuum system.

The system (see Figure 1) includes the following components:

- A source of a parallel visible light beam of sufficient diameter,
- The nominally axisymmetric mirror under test,
- A prism that has (1) reflective conical faces with angles and diameter suitably matched to the mirror under test and (2) an axis of symmetry nominally parallel to the light beam,
- A focusing lens, and
- A screen or a charge-coupled-device video camera, located at the nominal focal plane, that captures the image formed by the prism, the mirror under test, and the focusing lens.

The image on the focal plane consists of three components: Component 1 is nominally a point image formed by focusing of that part of the incident parallel light beam that passes directly through the lens. Component 2 is nominally a circular image formed by reflection of the incident light beam from the first conical surface of the prism, followed by reflection from the mirror under test, followed by reflection from the second conical surface of the prism, followed by focusing via the lens.

Component 3 nominally consists of one or more point image(s) formed by passage of part of the incident parallel beam through the central part of the prism and then through the lens. The precise nature of component 3 depends on the specific design of the entrance and exit faces of the central part of the prism: If, for example, the prism is made of optical glass with flat entrance and exit surfaces, then depending on the precision of parallelism between these surfaces, the resulting single point image may or may not coincide with the point image of beam 1. If, for another example, the prism is made of a metal, then the central core of the prism can be drilled out and a glass refractor with, say, three facets can be inserted to refract the incident parallel beam into three detected beams that, in turn, are focused to three point images on the screen (see Figure 2). These point images, in conjunction with the component-1 point image, can be used as fiducial marks for monitoring the orientation of the prism with respect to the incident parallel beam.

Among the most important features of this system are that the parallel light beam is the sole reference for the entire setup and the system inherently provides fiducial marks for its own alignment: The parallel light beam defines the direction of the optical axis. Once the axis of symmetry of the conical prism has been made parallel to the incident light beam and its position fixed, then the optical axis of the entire setup is fixed. The positions of the three

component-3 point images with respect to the single component-1 point image serve as real-time indications of the alignment of the axis of symmetry of the prism.

When the optical axes of the conical prism and the mirror under test and the conical prism are perfectly aligned with each other, and provided that the mirror under test is perfect, then the image on the focal plane is as shown in the upper part of Figure 2. If these two optical axes do not coincide and/or if the mirror under test is not perfect, then the image becomes distorted, as shown by example in the lower part of Figure 2.

This work was done by William W. Zhang of **Goddard Space Flight Center.** *Further information is contained in a TSP [see page 1].*
GSC-14365

Portable Instrument Detects Very Dilute Airborne Organics

This instrument offers an attractive alternative to GC/MS.

NASA's Jet Propulsion Laboratory, Pasadena, California

A small, lightweight, low-power instrument, denoted a proton-transfer-reaction/ion-mobility spectrometer (PTR-IMS) has been developed for detecting airborne organic compounds at concentrations in the sub-parts-per-billion range. Instruments like this one could be used on distant planets (such as Mars) to search for trace organic compounds indicative of life as well as numerous potential terrestrial uses: A few examples include medical applications (e.g., analyzing human breath to detect compounds associated with certain deadly diseases such as lung cancer and cirrhosis of the liver), law-enforcement applications (detecting airborne traces of explosives and drugs), environmental monitoring (detecting airborne pollutants and toxins), and military applications (detecting chemical warfare agents).

Portable gas-chromatography/mass-spectrometry (GC-MS) instruments that have commonly been used heretofore for detecting airborne organic compounds are characterized by three major shortcomings: (1) insufficient sensitivity for detecting sub-parts-per-billion concentrations, (2) susceptibility to undesired fragmentation of large organic molecules, and (3) the need for high vacuum and for high-vacuum equipment, which contributes greatly to size, weight, and mechanical complexity. In contrast, the PTR-IMS offers sensitivity adequate for detecting concentrations at the parts-per-billion level; operates in such a manner as not to fragment large organic molecules; and requires only a partial vacuum that can be generated by equipment smaller, lighter, and less complex than that needed for GC/MS.

The PTR-IMS includes a hollow-cathode ionizer, HCI (see figure), that is designed to generate reactant ions (RH^+, where R is a reactant molecule) and to exploit a proton-transfer reaction. The HCI operates at a pressure in the approximate range of 1 to 5 torr (≈ 0.1 to 0.7 kPa). H_2O is introduced into the discharge region inside the HCI, giving rise to the proton-transfer reaction

The Hollow-Cathode Ionizer generates reactant ions which then ionize target organic species. The target ions are then analyzed in the ion-mobility spectrometer.

$$RH^+ + M \rightarrow MH^+ + R,$$

where M is the target molecule and MH^+ is the desired product ion. R is chosen to be a molecule that has a proton affinity slightly less than that of M, in which case the probability for fragmentation channels of the proton-transfer reaction is low and the process of "soft" ionization is dominant. Moreover, the reaction is highly selective: Molecules that have proton affinities lower than that of R do not enter the reaction. H_3O^+ is the most suitable proton-donor reactant ion for investigating trace chemical species in either Martian or Earth air because H_3O^+ does not react with CO_2, CO, H_2O, O_2, N_2, He, Ne, Ar, or Xe.

The ions produced by the HCI are introduced along with a sample of air into a reaction chamber. Product ions generated in the reaction chamber are detected and analyzed in the IMS, which was chosen over conventional mass spectrometers and other instruments because it offers the sensitivity needed for detection in the sub-part-per-billion range, can handle a wider range of molecules, and does not require a high vacuum (it can even operate at normal terrestrial atmospheric pressure). In the IMS, a bias voltage produces an electric field that causes the reactant and product ions to drift in a desired direction. At the downstream end of the drift region, ions are detected by use of a high-gain electrometer; typically, the detected ion current can be on the order of a picoampere. A microprocessor controls the operation of the instrument and the acquisition, processing, and display of data.

In order to enable the determination of drift velocities, the ions are introduced into the drift region in pulses at time intervals typically between 20 and 40 ms. Within the drift region, the ions undergo spatial separation based on both mass and shape. For a given electric-field strength, the drift velocity of a given ion species is directly proportional to its specific mobility. Smaller ions tend to travel faster. By measuring the ion-drift times under a particular set of conditions, one can construct ion-mobility tables that can be used for identification of unidentified target ion species.

This work was done by Isik Kanik and Luther Beegle of Caltech for NASA's Jet Propulsion Laboratory. Further information is contained in a TSP [see page 1].

In accordance with Public Law 96-517, the contractor has elected to retain title to this invention. Inquiries concerning rights for its commercial use should be addressed to

Intellectual Property group
JPL
Mail Stop 202-233
4800 Oak Grove Drive
Pasadena, CA 91109
(818) 354-2240

Refer to NPO-21187, volume and number of this NASA Tech Briefs issue, and the page number.

Electrochemical Systems Generate Ozone and Ozonated Water

The only inputs needed are electric energy and mildly pressurized water.

Lyndon B. Johnson Space Center, Houston, Texas

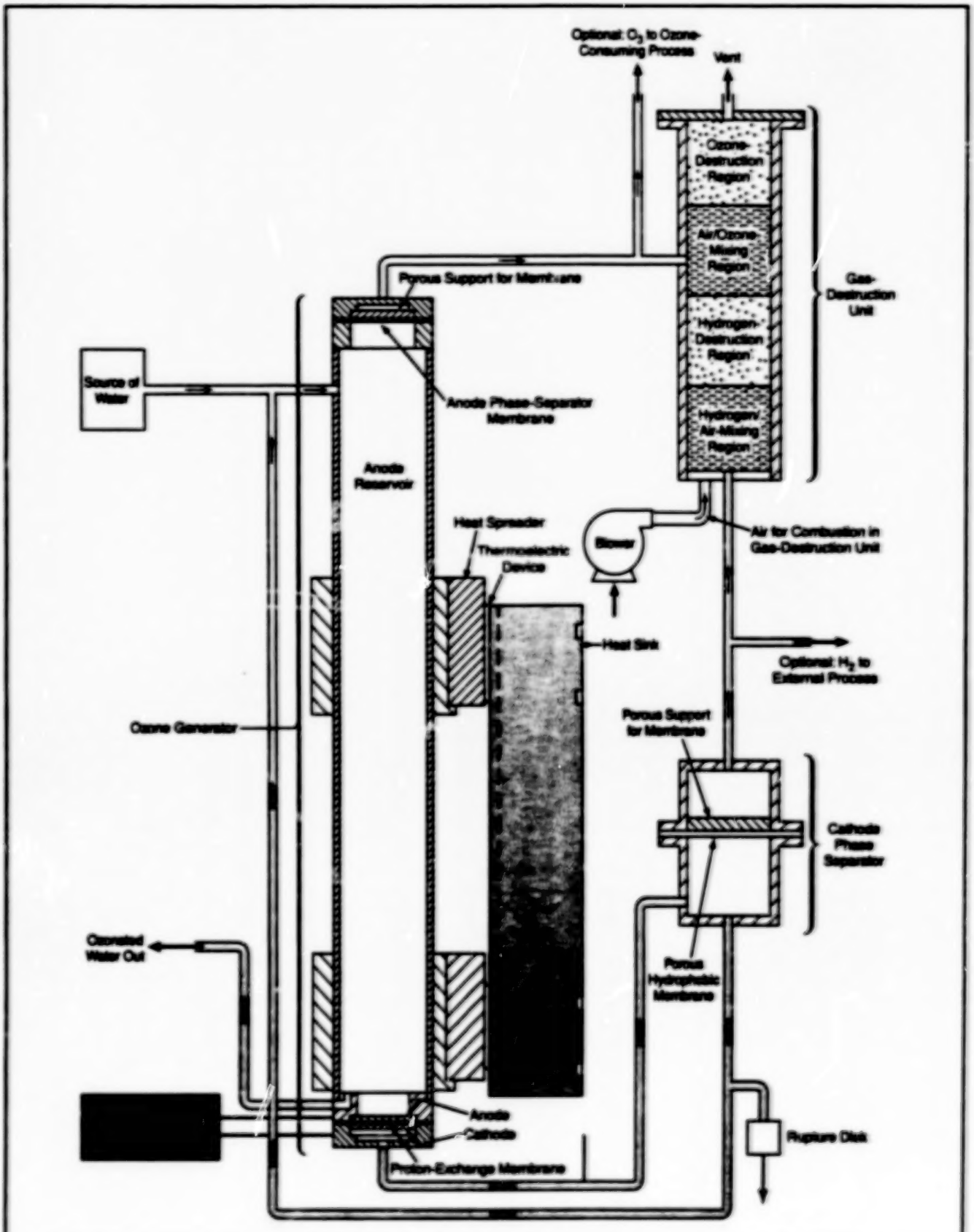

This System Adds Dissolved Ozone to a stream of water. The system also generates hydrogen and O_2/O_3 mixture as optional byproducts.

Improved electrochemical systems for generating ozone (in gaseous form and/or dissolved in water) have been invented for use in disinfection and in industrial processes in which the unique, highly oxidizing chemical properties of ozone are needed. More accurately, these systems generate oxygen along with high (relative to prior systems) concentrations of ozone and, optionally, with hydrogen as a byproduct. These systems contain no pumps and very few moving or wearing components, and the only inputs needed to operate these systems are electric energy and water supplied at mild pressure. Moreover, these systems can readily be designed and constructed on any scale (e.g., from research laboratory to industrial) to suit a wide variety of applications.

A basic system of this type (see figure) includes a power supply, an ozone-generator/anode-reservoir unit, a cathode phase separator, and a gas-destruction unit. At the bottom of the anode reservoir lies the active part of the ozone generator, which preferably is an electrolytic cell that contains a proton-exchange membrane with a porous anode on its upper face and a porous cathode on its lower face. A catalyst on the anode promotes the electrolytic production of oxygen and ozone, some of which dissolves into the water in the anode reservoir. The anode reservoir also serves as part of a liquid/gas separator, wherein oxygen and ozone generated at the anode form into bubbles or diffuse from the water and rise to the top of the reservoir. The rest of this phase separator is a hydrophobic membrane at the top of the reservoir that allows the O_2 and O_3 gases, but not water, to pass through to the top side. The mixture of O_2 and O_3 gases can be fed either to an O_3-consuming process or to the gas-destruction unit.

A tube connects the cathode with the cathode phase separator. A hydrophobic membrane in the cathode phase separator allows hydrogen gas, but not water, to pass through to the top side. Hydrogen gas from the dry (top) side of the membrane is either sent to the gas-destruction unit or discharged to a hydrogen-consuming external process. Preferably, water that has been transferred from the anode to the cathode by electroosmosis is returned from the bottom of the cathode phase separator to the input (top) end of the anode reservoir through the tube depicted as the longest in the figure.

The source of water is connected directly to the anode reservoir. The liquid/gas-separator membranes make it possible for the water from the source to displace any gases from anode reservoir and from the lower compartment of the anode phase separator. Once these gases have been displaced, the water comes into direct contact with these membranes and the transfer of water ceases as the pressures in the anode reservoir and cathode phase separator equalize with the pressure in the source of water. Provided that the pressure in the source equals or exceeds the pressure in the anode reservoir, the anode reservoir and the cathode phase separator remain full of water during all phases of operation.

Preferably, a cooling unit (e.g., comprising heat spreaders, thermoelectric devices, and a heat sink) is attached to the anode reservoir to remove waste heat and to chill the reservoir in order to reduce the rate of degradation of dissolved ozone and increase the solubility of ozone in the water. The output stream of ozonated water is taken from just above the anode at the bottom of the anode reservoir.

The gas-destruction unit includes a source of combustion air, a hydrogen/air-mixing region, a hydrogen-destruction zone that contains a hydrogen/air-combustion catalyst, an air/ozone-mixing region, and an ozone-destruction region that contains an ozone-destruction catalyst. The products of the gas-destruction unit are vented and/or drained.

This work was done by Oliver J. Murphy, Craig C. Andrews, and Thomas D. Rogers of Lynntech, Inc., for **Johnson Space Center.**

In accordance with Public Law 96-517, the contractor has elected to retain title to this invention. Inquiries concerning rights for its commercial use should be addressed to

Lynntech, Inc.
7610 Eastmark Drive
Suite 202
College Station, TX 77840
Tel. No: (409) 693-0017
Fax No: (409) 764-7479

Refer to MSC-23046, volume and number of this NASA Tech Briefs issue, and the page number.

Liquid-Crystal Phase-Shifting Shearing Interferometer

There is no need for critical alignment or focus adjustment.

John H. Glenn Research Center, Cleveland, Ohio

The liquid-crystal phase-shifting shearing interferometer is a common-path interferometer based partly on a lateral-shear-plate interferometer. It bears a partial similarity to the liquid-crystal point-diffraction interferometer (LCPDI), which is also of the common-path type. The phase-shifting nature of this interferometer is expected to increase (relative to prior shearing interferometers) resolution by up to two orders of magnitude. The liquid-crystal phase-shifting shearing interferometer is expected to be useful for measuring spatially varying optical density in a laboratory or manufacturing setting; examples of such densities include the index of refraction of a liquid in a production process, the density and/or temperature of a gas in a combustion system, and the temperature of a fluid in a boiler.

The proper functioning of the LCPDI depends on focusing a laser beam onto a transparent microsphere and, hence, depends on the critical adjustment of a focusing lens by a highly trained technician. Unlike the LCPDI and many other interferometers, the liquid-crystal phase-shifting shearing interferometer can be aligned easily, with no need for critical adjustments by a highly trained technician. Moreover, elimination of the need for focusing on a microsphere also eliminates phase noise associated with inhomogeneities in a focusing lens.

In the liquid-crystal phase-shifting shearing interferometer, collimated light from a laser is incident on a shear plate oriented at an angle of 45° (see figure). Unlike a traditional shear plate, this shear plate contains a liquid-crystal layer that can be used to vary the phase of the light reflected from its rear surface. The amount of shear depends on the effective optical thickness of the shear plate, which is comparable to the combined optical thicknesses of its glass layers. When a voltage is applied across the liquid-crystal layer, the index of refraction of the layer changes, causing the phase of the portion of the incident light reflected from the rear surface to be stepped relative to the phase of this portion when the voltage is not present. Calibration of the phase shift as a function of voltage can produce the phase steps required to implement common phase-stepping algorithms.

The amount of shear varies roughly inversely with index of refraction and thus with the phase. However, calculations for the case of a total shift of one wavelength have shown that the total shift in beam position can be safely neglected because it is more than an order of magnitude below the size of a typical pixel in a charge-coupled-device camera that would be used in

implementing a practical version of this interferometer.

In a prototype of this liquid-crystal phase-shifting shearing interferometer, the shear plate is a commercial liquid-crystal phase retarder originally intended for use as an extended-range, variable-retardance wave plate rather than an interferometer component. The manufacturer's specification for reflectance at each surface is less than half of one percent. The device would perform optimally if its front surface were coated with a partially reflective film and its rear surface with a totally reflecting film.

This work was done by DeVon W. Griffin of **Glenn Research Center**. *Further information is contained in a TSP [see page 1].*

Inquiries concerning rights for the commercial use of this invention should be addressed to NASA Glenn Research Center, Commercial Technology Office, Attn: Steve Fedor, Mail Stop 4–8, 21000 Brookpark Road, Cleveland, Ohio 44135. Refer to LEW-17165.

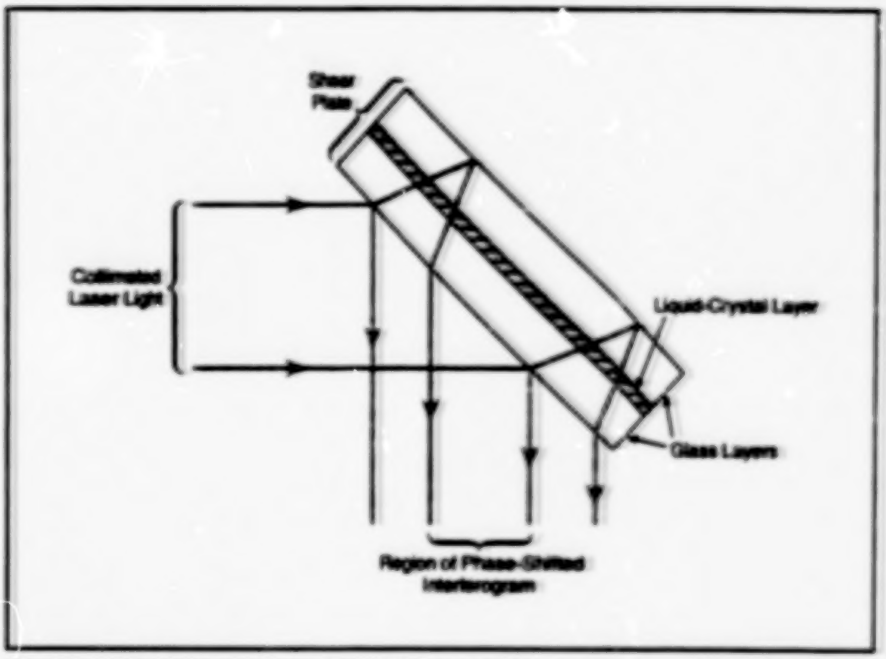

The Liquid-Crystal Layer in the Shear Plate is used to vary the phase of the light reflected from its rear surface.

Phase-Retrieval Camera for Optical Testing

Effects of vibrations and turbulence are removed with the help of a fast shutter.

A portable instrument denoted a phase-retrieval camera (PRC) is designed to enable the testing of large, lightweight optics in the presence of vibrations and atmospheric turbulence. The development of the PRC was prompted by the fact that conventional optical-testing techniques are not sufficiently accurate or robust for optical testing in high-vibration environments.

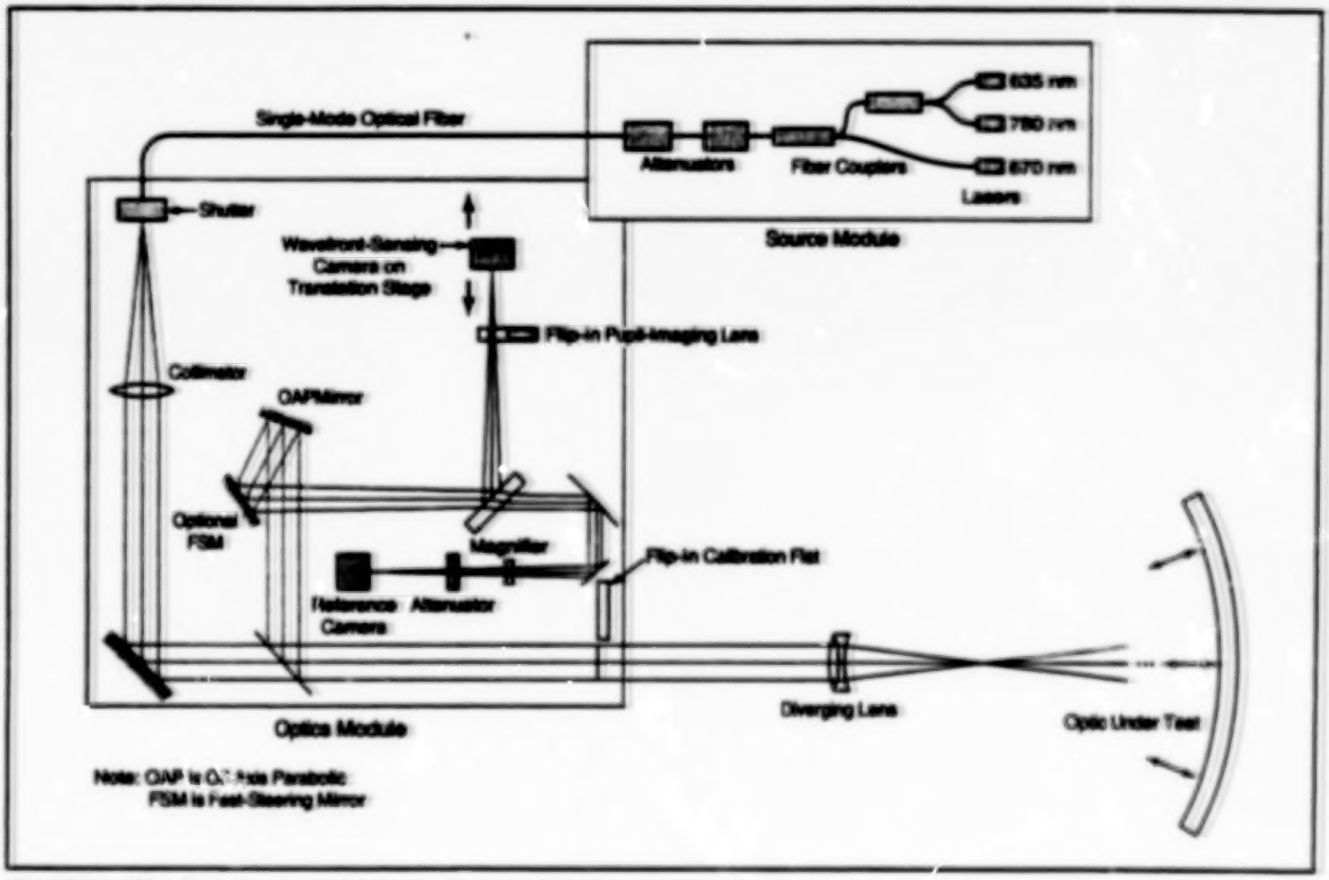

The PRC in This Example of a typical application is used to test a concave mirror.

The PRC (see figure) includes a source module and an optics module. The source

module contains laser diodes and integrated optical devices that, acting together, constitute a point source of light of three wavelengths. The use of the three wavelengths makes it possible to measure the relative axial displacement (called "piston" in the art) of a segment of an optic under test. The optics module contains a wavefront-sensing (phase-retrieval) camera on a motorized translation stage, a reference (boresight) camera, a short-exposure (millisecond) shutter to "freeze" vibrations and turbulence, selectable calibration optics, attenuators, and other optics. A defocused image of the optic under test is formed on the focal plane of the wavefront-sensing camera.

The PRC also includes a computer programmed with software that provides a graphical user interface, displays data, controls the operation of the instrument, enables data communication and remote control via the Internet, and performs phase-retrieval, phase-unwrapping, and calibration computations. The phase-retrieval algorithm processes multiple short-exposure images from the wavefront-sensing camera and aligns them with each other by use of boresight calibration images acquired simultaneously by the reference camera. The algorithm generates data and imagery that characterize the wavefront generated by (and thus the surface figure of) the optic under test.

This work was done by David Redding, Andrew Lowman, David Cohen, Fang Shi, and Scott Basinger of Caltech for **NASA's Jet Propulsion Laboratory**. *Further information is contained in a TSP [see page 1].*
NPO-21217

Solar Simulator for a Portable Solar-Absorptance Instrument

The principal advantages are portability and accurate normalized AM0 spectrum.

John F. Kennedy Space Center, Florida

A special-purpose solar simulator includes (1) a tungsten lamp that serves as a gray-body radiator with a temperature of 3,200 K and (2) a mosaic of filters such that the filtered lamp output has the same normalized spectral irradiance as that of sunlight outside the atmosphere of the Earth. This solar simulator is intended for use as the illuminator in a portable instrument that measures solar absorptances and total emittances of samples of materials.

The extra-atmospheric sunlight spectrum [also known as the airmass zero (AM0) spectrum] in question is the one described in standard E490-73a of the American Society for Testing and Materials (ASTM). The present solar simulator was developed because previously developed solar simulators are unsuitable for a variety of reasons: some do not cover the wavelength range (300 to 2,800 nm) required in the design specification for the instrument, some are too power-hungry and/or not durable enough for inclusion in a portable instrument, and some deviate too much from the ASTM standard.

The mosaic of filters includes commercially available filters plus a keystone filter developed specifically for this application. The mosaic was designed by use of a mathematical model based on the transmittance characteristics of the filters. The model was evaluated against optical "bread board" measurements. Areas, overlaps, and other design parameters were determined for the finished filter configuration.

A prototype instrument was built for proof of design. All design specifications relating to the filter were met: The filtered lamp output covers the spectral range from 300 to 2,800 and agrees more than 95 percent with the ASTM standard sun. Solar-absorptance measurements taken by the instrument are characterized by errors with magnitudes of less than 3 percent (that is, within a range of ±3 percent) of total absorptance.

The major benefit afforded by the design of this solar simulator is portability arising from low power consumption (relative to other solar simulators) and robustness. In addition, the compactness of the solar simulator (relative to other solar simulators) made it possible to integrate both the measurement of solar absorptance and the measurement of emittance into a single instrument package, whereas it would otherwise have been necessary to package them as separate instruments. Other benefits afforded by the design of the overall instrument are that a measurement can be made in <1 minute, and the instrument is more economical than are spectroradiometric systems.

The original intended use of the instrument is in measuring the radiative properties of components of the International Space Station. The instrument could also be used to measure the radiative properties (especially with respect to thermal radiation) of coatings and other materials, particularly in the aerospace industry.

This work was done by David G. Crandall and John S. Harchanko of AZ Technology, Inc., for **Kennedy Space Center**.
KSC-12069

Books and Reports

Quantum Mechanics of Harmonic Oscillator in External Fields

A report presents a theoretical study of a harmonic oscillator in homogeneous or nonhomogeneous externally applied electric and/or gravitational fields. The standard quantum-mechanical formalism for a simple harmonic oscillator, starting with the Hamiltonian and the associated creation and annihilation operators, is modified to incorporate the additional terms representing the external fields. The correspondingly modified solutions of the Schroedinger equation are derived. It is shown that an applied homogeneous field does not change the frequency of the oscillator but does change its equilibrium position, and that an applied inhomogeneous field changes both the frequency and the equilibrium position. The formalism thus developed is used to calculate the partition function of a low-temperature gas of fermions that are trapped in the harmonic-oscillator field and that interact with the externally applied field(s) but not with each other. Then equations for the thermodynamic potential and the internal energy of, and the number of fermions in, the gas are derived from the partition function. These equations show how the thermodynamic properties of the Fermi gas depend on the external fields.

This work was done by Igor Kulikov of Caltech for **NASA's Jet Propulsion Laboratory**. *To obtain a copy of the report, "Harmonic oscillator in external fields: Theory and applications," see TSP's [page 1].*
NPO-30262

Effect of Gravitation on Noninteracting Trapped Fermions

A report presents a theoretical study of the thermodynamics of an ultralow-temperature gas of fermions that interact with a gravitational field and with an externally imposed trapping potential but not with each other. The gravitational field is taken to define the z axis and the trapping potential to be of the form $(m/2)(\omega_x x^2+\omega_y y^2+\omega_z z^2)$, where m is the mass of a fermion; x, y, and z are Cartesian coordinates originating at the center of the trap; and the ω values denote effective harmonic-oscillator angular frequencies with respect to motion along the respective coordinate axes. The single-particle energy is found from the solution of the time-dependent Schroedinger equation for a Hamiltonian that includes kinetic energy plus the gravitational and trapping potentials. The equation for the single-particle energy is combined with Fermi statistics to obtain equations for the chemical potential, internal energy, and specific heat of the gas; the number of trapped fermions; and the spatial distribution of fermions at zero temperature. The equations reveal the ways in which the Fermi energy, the specific heat, and the shape of the Fermion cloud are affected by the gravitational field and the anisotropy of the trapping field.

This work was done by Igor Kulikov of Caltech for **NASA's Jet Propulsion Laboratory**. *To obtain a copy of the report, "An influence of gravitational field on properties of trapped fermions," see TSP's [page 1].*
NPO-30248

BLANK PAGE

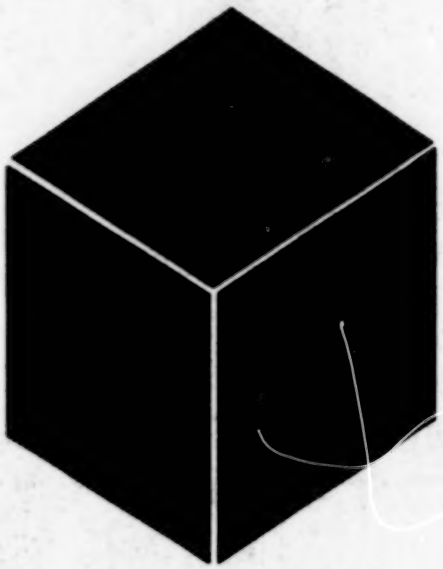

Materials

Hardware, Techniques, and Processes

33 Protective Solid Electrolyte Films for Thin Li-Ion Cells

Protective Solid Electrolyte Films for Thin Li-Ion Cells

These films would simplify fabrication and afford greater flexibility in design.

NASA's Jet Propulsion Laboratory, Pasadena, California

Thin films of Li_2CO_3 are under consideration for use as passivating layers between electrodes and solid electrolytes in advanced thin-film lithium-ion electrochemical cells. By suppressing undesired chemical reactions as described below, the Li_2CO_3 films could help to prolong the shelf lives, increase the specific energies, and simplify the fabrication of the cells. Batteries comprising one or more cells of this type could be used as sources of power in such miniature electronic circuits as those in "smart" cards, implantable electronic medical devices, sensors, portable communication devices, and hand-held computers.

The need for passivation arises as follows:

- A state-of-the art thin-film Li-ion cell typically consists of a lithium metal anode, a glassy solid electrolyte, and a cathode made of a lithiated transition-metal oxide (e.g., $LiCoO_2$). The Li anode and most solid electrolytes are very sensitive to humidity. To prevent destruction of the anode and solid-electrolyte films by reactions with airborne moisture, it is necessary to adhere to strict handling procedures during fabrication; in particular, the electrode and electrolyte films must be handled in a glove box. As a consequence, the overall process of fabrication of thin-film Li-ion cells and batteries is more complex than it would otherwise be.
- Many solid electrolytes are not chemically or electrochemically stable when in contact with Li or when exposed to high charging potentials. Intermediate passivating films that could protect such solid electrolytes at the anode and cathode potentials would be very desirable.

The selection of materials for thin-film Li-ion batteries involves concerns similar to those for conventional bulk Li-ion batteries. However, the techniques used to fabricate thin-film batteries offer distinct advantages over those used to fabricate conventional batteries by affording the flexibility to design cells with multilayer thin-film structures that can be made to exhibit properties not attainable in bulk structures. As an especially relevant example, a thin-film electrolyte structure can comprise a film of a high-ionic-conductivity material coated with a film of a material of lower ionic conductivity but greater stability versus Li. The development of films that can provide stability at anode and cathode potentials enables the use of many electrolyte materials, including both novel electrolytes and electrolytes that were known previously and were considered unusable because of poor chemical or electrochemical stability.

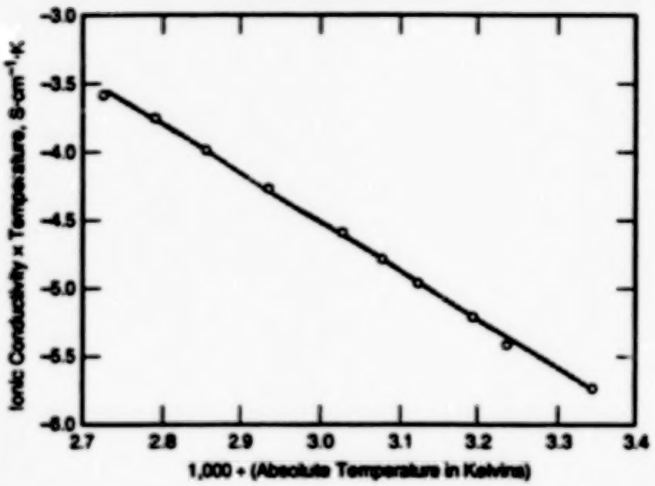

An Arrhenius Activation Curve with a relatively low activation energy of <0.35 eV appears to be consistent with the temperature dependence of the measured ionic conductivity of Li_2CO_3.

Li_2CO_3 is electronically insulating and somewhat ionically conductive. In research conducted thus far, solid electrolyte films of Li_2CO_3 have been prepared by magnetron sputtering. These films have been found to be stable in air and to be useful for protecting components of Li-ion cells as described above. More specifically, the Li_2CO_3 films have been found to afford (1) excellent passivation against reactions between electrolytes and anodes; (2) excellent stability against oxidation at high voltage, as evidenced by the oxidative stability of carbonate-based liquid electrolytes at potentials up to 4.8 V, and (3) a high degree of stability in presence of humidity. The resistance to attack by airborne moisture is an important advantage in that during fabrication, air-sensitive components passivated by Li_2CO_3 can be moved between processing tools in ambient air.

In impedance-spectroscopy tests, Li_2CO_3 films sandwiched between Mo electrodes exhibited electrical characteristics similar to those of other solid electrolyte films. The room-temperature ionic conductivity of the $LiCoO_2$ was found to be rather poor ($\approx 5 \times 10^{-9}$ S/cm), though it was found to fit to an Arrhenius activation curve (see figure). Given this low ionic conductivity, Li_2CO_3 would likely not be suitable for main electrolyte layers, but would be better suited for thin passivating films.

This work was done by Ratnakumar Bugga and William West of Caltech for **NASA's Jet Propulsion Laboratory.** *Further information is contained in a TSP [see page 1].*

NPO-20953

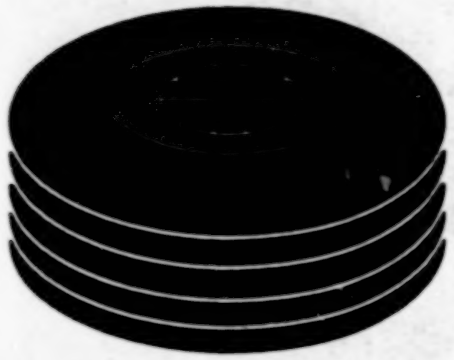

Computer Programs

Physical Sciences

37 Updated Global Atmospheric Reference Model Computer Programs
37 Software Automates Processing of SAR Image Data
38 Program for International-Temperature-Scale Calculations

Mechanics

38 Gyroscope Automated Testbed

Mathematics and Information Sciences

38 Multi-Screen-Image- and Catalog-Viewing Program
38 Program Improves Transfer of Data From CAD to Machine Shops

Physical Sciences

Updated Global Atmospheric Reference Model Computer Programs

The 1999 version of the NASA/Marshall Space Flight Center Global Reference Atmospheric Model (GRAM-99) and version 3.8 of the Mars Global Reference Atmospheric Model (Mars-GRAM) are the latest in two series of computer programs for calculating selected physical properties of the atmospheres of Earth and Mars, respectively. GRAM-99, like prior versions of GRAM, implements an amalgamation of empirical models that represent geographical, seasonal, and monthly variations of the state of the terrestrial atmosphere (thermodynamic variables and horizontal and vertical wind components) at all altitudes from the ground up to those of spacecraft orbits. Mars-GRAM provides engineering estimates of density, temperature, pressure, and wind components in the Martian atmosphere as functions of latitude, longitude, altitude, and time.

The 1995 version of GRAM (GRAM-95) and the underlying model were described in "NASA/MSFC Global Reference Atmospheric Model — 1995 Version" (MFS-31105) *NASA Tech Briefs*, Vol. 21, No. 3 (March 1997), page 68. For altitudes from 0 to 27 km, GRAM-99 utilizes either of two sets of data: the binary-formatted Global Upper Air Climatic Atlas (GUACA) [which was also used in GRAM-95] or the newer ASCII-formatted Global Gridded Upper Air Statistics (GGUAS). For altitudes from 20 to 120 km, GRAM-99 uses, as did GRAM-95, a specially developed set of data based on Middle Atmosphere Program (MAP) data. Above 90 km, GRAM-99 uses the 1999 version of the Marshall Engineering Thermosphere (MET) model [also known as the Jacchia model]. Fairing techniques assure smooth transitions among the models and sets of data in the overlap height ranges of 20 to 27 km and 90 to 120 km.

Like GRAM-95, GRAM-99 estimates concentrations of water vapor and of O_3, N_2O, CO, CH_4, CO_2, N_2, O_2, O, A, He, and H. For altitudes above 90 km, the Jacchia model can also provide concentrations of N_2, O_2, O, A, He, and H. Atmospheric-constituent profiles of the Air Force Geophysics Laboratory are also used extensively for altitudes up to 120 km.

GRAM-95 incorporated a then new variable-scale perturbation model that provides both large-scale (wave) and small-scale (stochastic) deviations from mean values for thermodynamic variables and horizontal and vertical wind components. Such perturbations are characterized by time scales of less than a month and are associated with turbulence, storms, atmospheric tides, and other phenomena. GRAM-99 incorporates improvements in the small-scale perturbation model for representing intermittent phenomena.

A major new feature in GRAM-99 is an option to substitute Range Reference Atmosphere (RRA) data for conventional GRAM climatological data when a trajectory passes sufficiently near any RRA site. This feature makes it possible, for example, to simulate the atmosphere, starting from takeoff at one RRA site (e.g., Edwards Air Force Base), where RRA data are used, then make a smooth transition to an atmosphere characterized by GRAM climatology en route, then make another smooth transition to an atmosphere characterized by RRA data at a landing site (e.g., White Sands, New Mexico).

A complete user's guide for running GRAM-99 is available. The user's guide includes sample input and output. Also included is an example that shows how to incorporate GRAM-99 as a subroutine in another program (e.g., a trajectory code).

Mars-GRAM implements a mathematical model based on surface and atmospheric measurements taken during the Mariner and Viking (orbiter and lander) missions. At altitudes above about 120 km, the Mars-GRAM model is based on the Stewart (1987) Mars thermospheric model. Mars-GRAM can be used as a stand-alone program or can be incorporated into an orbit-propagator or trajectory code.

Version 3.8 of Mars-GRAM incorporates some new features that were suggested by users engaged in the design and operation of spacecraft on missions of robotic exploration of Mars. Mars-GRAM 3.8 uses new values of planetary reference ellipsoid radii, gravitation terms, and the rate of rotation, (consistent values now used by NASA's Jet Propulsion Laboratory), and includes centrifugal effects on gravity. The model now uses the NASA Ames Global Circulation Model low-resolution topography. Curvature corrections are applied to winds, and limits based on speed of sound are applied. The altitude and molecular weight of the ionization peak of the F1 layer of the Martian ionosphere and the density scale height (including the effects of the change of molecular weight with altitude) are computed. A check is performed to disallow temperatures below the sublimation temperature of CO_2.

The user's guide for Mars-GRAM 3.8 summarizes the changes made for this version and includes an appendix that summarizes changes made for versions 3.5 through 3.7. It includes instructions for running the program, plus sample input and output files.

These programs were written by Carl G. Justus of Computer Sciences Corp. for **Marshall Space Flight Center**. *For further information, contact Carl G. Justus at Jere.Justus@msfc.nasa.gov.*
MFS-31461/62

Software Automates Processing of SAR Image Data

The Automated SAR Image Processor (ASIP) computer program increases the efficiency of production of scientifically useful imagery from raw synthetic-aperture-radar (SAR) image data. In the absence of ASIP, the processing of SAR data is a labor-intensive task, often involving supporting personnel, that requires expertise in the use of a variety of image-data-processing programs, as well as expertise in the scientific specialty of the end user. ASIP captures the diverse components of expertise to assist the scientific end user in obtaining the scientific end product without supporting personnel. ASIP applies artificial-intelligence planning techniques to reason about the interactions and interfaces among the many specialized programs needed to process SAR data. The planning component of ASIP then manages the flow of information and control in order to produce the desired scientific data product efficiently. In one application, for example, ASIP made it possible to produce special maps pertaining to the study of surface winds with only 1/10 the number of manual inputs and 30 percent less central-processing-unit time than would otherwise be necessary.

This program was written by Steve Chien, Forest Fisher, Ronald Greeley, and Edisanter Lo of Caltech for **NASA's Jet Propulsion Laboratory**. *Further information is contained in a TSP [see page 1].*

This software is available for commercial licensing. Please contact Don Hart of the California Institute of Technology at (818) 393-3425. Refer to NPO-20509.

Program for International-Temperature-Scale Calculations

A computer program implements several aspects of the International Temperature Scale of 1990 (ITS90).

- For platinum resistance thermometers (PRTs), the program can perform reference-function (W_{ref}) calculations traceable to the National Institute of Standards and Technology (NIST) through its Technical Note 1265. W_{ref} represents a perfect PRT that has a resistance of exactly 1 Ω at the triple-point temperature of water. The program provides for the entry of coefficients generated by a calibration facility and converts a measured resistance to an equivalent temperature with an accuracy of 5 millikelvins. The program also performs measurement calculations for PRTs: In such a calculation, the triple-point temperature of water as determined by a calibration laboratory is multiplied by the applicable NIST reference value.
- The program converts between output voltages and temperatures for several types of thermocouples that yield measurements traceable to NIST through its Monograph 175. These thermocouples are of types T (Cu/Cu-Ni), K (Ni-Cr/Ni-Al), J (Fe/Cu-Ni), E (Ni-Cr/Cu-Ni), N (Ni-Cr-Si/Ni-Si-Mg), B [Pt(30 percent)-Rh/Pt(6 percent)-Rh], S [Pt(10 percent)-Rh/Pt], and R [Pt(13 percent)-Rh/Pt].

This program was written by Richard T. Deyoe of Dynacs, Inc., for **Kennedy Space Center**. *Further information is contained in a TSP [see page 1].*
KSC-12166

Mechanics

Gyroscope Automated Testbed

The Gyroscope Automated Testbed (GAT) is a fully automated inertial device characterization testbed. Rotational response parameterization and short-term noise stability analysis are the fundamental principles behind the system. Complete response characterization, bias stability, sensitivity, and range are supported along with a drift stability and noise analysis through use of a Green chart and calculation of the power spectral density. GAT is also capable of performing turn-on cycle stability and temperature-dependent testing.

The system is fully automated yet allows complete customization of test parameters. Each of the specific tests may be enabled or disabled as desired, and each test may be individually configured. The state of the system can be saved and loaded at any time providing quick and easy access to various configurations.

The hardware interface layer of the program has been abstracted to provide a flexible yet robust method of input and control. The data-acquisition subsystem provides a universal method of acquiring data from devices. Direct analog inputs are provided and can be individually customized. General-purpose-interface-bus- (GPIB-) compliant devices may be used for either input (i.e., voltmeters) or as control or output (i.e., temperature controller). This flexible arrangement allows nearly unlimited expandability and extendibility to future capabilities. An abstract rate table interface permits control of any rate table which supports an analog or GPIB interface.

Results are presented in both summary and complete form. Processed and raw data can be saved to a file during a test. Key values and data plots are output to a table in real time during a test. At the completion of a testing session, a document is automatically generated which summarizes the results and encapsulates all output charts generated during the session.

The GAT system provides a cost-effective way of characterizing inertial devices. Although designed for analyzing micro-electromechanical (MEMS) vibratory gyroscopes, it can easily be adapted to accelerometers by simply changing the units of measure. It is also highly efficient as up to five devices can be tested simultaneously.

The GAT system currently is executed on a Pentium III (or equivalent), 550-MHz computer with 256MB of RAM, 10GB hard drive, internal data acquisition card, and GPIB interface card.

This program was written by Christopher Evans and Roman Gutierrez of Caltech for **NASA's Jet Propulsion Laboratory**. *Further information is contained in a TSP [see page 1].*

This software is available for commercial licensing. Please contact Don Hart of the California Institute of Technology at (818) 393-3425. Refer to NPO-20847

Mathematics and Information Sciences

Multi-Screen-Image- and Catalog-Viewing Program

A computer program enables the single- or multi-screen display of multispectral, multiresolution images — especially astronomical ones — stored as sets of data that range upward in size from hundreds of gigabytes. In cases of multi-screen displays, the software synchronizes the screens so that they act as a single ultrahigh-resolution display. It is possible to pan and zoom smoothly to any part of the data at any resolution. The software can automatically generate composites of multiple sets of data, making it possible, for example, to overlay high-resolution insets on background images or to display a separate source image for each video channel (red, green, or blue). The software includes special features to aid viewing of astronomical data: these include a capability for displaying catalogs as ASCII text or as image overlays, and a catalog-to-image relational capability that enables the user do such things as select a region of the image and view those objects in the region that are highlighted in both the image and in the catalog. Alternatively, when an object in the catalog is selected, the user can see that object highlighted in the image or can jump to the position of the object in the image.

This program was written by Joseph Jacob of Caltech for **NASA's Jet Propulsion Laboratory**. *Further information is contained in a TSP [see page 1].*

This software is available for commercial licensing. Please contact Don Hart of the California Institute of Technology at (818) 393-3425. Refer to NPO-30132.

Program Improves Transfer of Data From CAD to Machine Shops

The EMNet computer program has been developed to overcome the difficulties and reduce the errors that, heretofore, have been encountered in transferring data from computer-aided design (CAD) systems to computer numerically controlled (CNC) machines. EMNet could improve operations in almost any industrial machine shop that uses CNC equipment.

The difficulties and errors in question arise because CNC output files (files of numerical control data generated by CAD postprocessing programs) have customarily been transferred either by use of floppy disks or by manual entry of data into CNC equipment. Sometimes these files are too large to fit on floppy disks. Even when floppy disks are used, data transfers often fail. Moreover, although some programs for transfer of data from CAD to CNC operations have been commercially available, those programs are expensive, are usable only by persons who have advanced computer skills, and have caused failures of computer networks.

EMNet was designed for use by machinists who have little or no computer experience and are responsible for entering numerical control data into CNC machinery, as needed, to produce machined parts. EMNet features an easy-to-use "point and click" graphical user interface, and is available in versions for the Windows 3.x, Windows 95, and Windows NT operating systems. EMNet offers a full complement of Windows-style help displays for both machinists and computer-workstation administrators.

A computer on which EMNet is executed communicates with CNC machines via RS-232 serial interfaces connected according to specifications of the manufacturers of the machines. EMNet is easily configurable, and can be executed on a personal computer connected to two CNC machines. Each CNC machine can be assigned a name, a communication port, a default directory for data files, and options for whether to transmit carriage returns, line feeds, or end-of-block characters to the machine. If two machines are connected to a computer, the communication protocol for each port can be configured for the corresponding machine, separately from the protocol for the other port and its machine. Both the machine options and the communication-port settings are protected by a password that can be changed by a computer-workstation administrator.

After EMNet has been configured, the interaction required by the machinist is minimal. To transmit numerical control data to a CNC machine, the machinist performs the following steps:

1. Choose the machine by use of front-panel option buttons in an EMNet display. EMNet automatically switches to the default directory for the machine and opens the respective communication port.
2. Click the "File" button on the EMNet display and select the file to transfer.
3. Prepare the CNC machine to receive the file.
4. Click the EMNet "Send" button.

To receive numerical control data from a CNC machine by use of EMNet, the machinist performs the following steps:

1. Choose "Settings," "Transfer," "Receive" from the EMNet menu.
2. Click the "Receive" button.
3. Send the data from the control panel of the CNC machine.

EMNet also offers the capability of performing a byte-by-byte comparison of two numerical-control-data files. This capability was added to ensure that the data received by a CNC machine are intact; that is, without errors or missing bytes. To initiate a byte-by-byte comparison, the machinist performs the following steps:

1. Choose "File," "Compare" from the EMNet menu.
2. Select the "known good" (original) file.
3. Select the file to compare (typically, a file transferred from a CNC machine back to the computer.
4. Verify whether the CNC machine includes a "program number" in the downloaded data, and if so, the line where the program number resides (typically line 2).

EMNet then performs a byte-by-byte comparison of the two files and displays the results. If a data mismatch is encountered, the comparison is terminated and the line and byte location of the mismatch is displayed.

This work was done by W. David Smith of Rothe Joint Venture, L.P., for **Johnson Space Center**.

MSC-22986

BLANK PAGE

Mechanics

Hardware, Techniques, and Processes

43 Study of Turbulent Boundary Layer on the F-15B Airplane
44 Improved Alignment Mechanism for Robotic Drilling
45 Measuring Volume of Incompressible Liquid in a Rigid Tank

Books and Reports

45 Algorithms for Collision-Avoidant Formation Flying
46 Improvements in a Piezoelectrically Actuated Microvalve
46 Low-Energy Transfer From Near-Earth to Near-Moon Orbit

BLANK PAGE

Study of Turbulent Boundary Layer on the F-15B Airplane

Automated hot-wire anemometry has been demonstrated in flight tests.

Dryden Flight Research Center, Edwards, California

NASA's F-15B #836 is a two-seat version of the F-15, which is a high-performance, supersonic, all-weather fighter airplane. The F-15B is used as a test-bed aircraft for a wide variety of flight experiments. In support of this use, a flight-test fixture (FTF) was developed to provide a space for flight experiments in a region with known aerodynamic conditions. The FTF is a fully instrumented test article mounted on the center line of the bottom of the fuselage of an F-15B airplane. The FTF includes an interchangeable experiment panel and is 107 in. (2.72 m) long, 32 in. (0.81 m) high, and 8 in.(20.3 cm) wide, with a 12-in. (30.5-cm) elliptical nose section. The FTF has been used in many flight experiments during the past several years and can be modified to satisfy a variety of research requirements.

One method of measuring turbulent fluctuations of density and velocity across the compressible boundary layer of an aircraft surface in flight (which fluctuations give rise to Reynolds stresses) involves the use of a recently developed automated hot-wire anemometry system. Prior to the development of the automated hot-wire anemometry system, a method of measuring turbulent velocity fluctuations in flight had not been perfected and routinely used in NASA's flight experiments, primarily because of the limitations of conventional anemometry systems. Conventional anemometry systems are characterized by difficulties in tuning, poor signal-to-noise ratios and low bandwidths at low overheat ratios, sensitivity to electromagnetic interference, and vulnerability to effects of cable capacitance. The automated hot-wire anemometry system is, more specifically, a constant-voltage anemometry (CVA) system that has been shown not to be subject to the aforementioned deficiencies of conventional anemometry systems. The CVA system was selected for flight testing on the FTF on the F-15B airplane.

It is essential to characterize the turbulent boundary layer in flight experiments because the length scales characteristic of turbulence in wind-tunnel experiments are significantly different from those of turbulence in flight. Thus, flight measurements in turbulent boundary layers are necessary for validation of computational fluid dynamics (CFD) computer codes and for predicting transitions from laminar to turbulent flow. The specific objective of the flight tests was to validate the concept of CVA for measuring velocity fluctuations in turbulent boundary layers in flight.

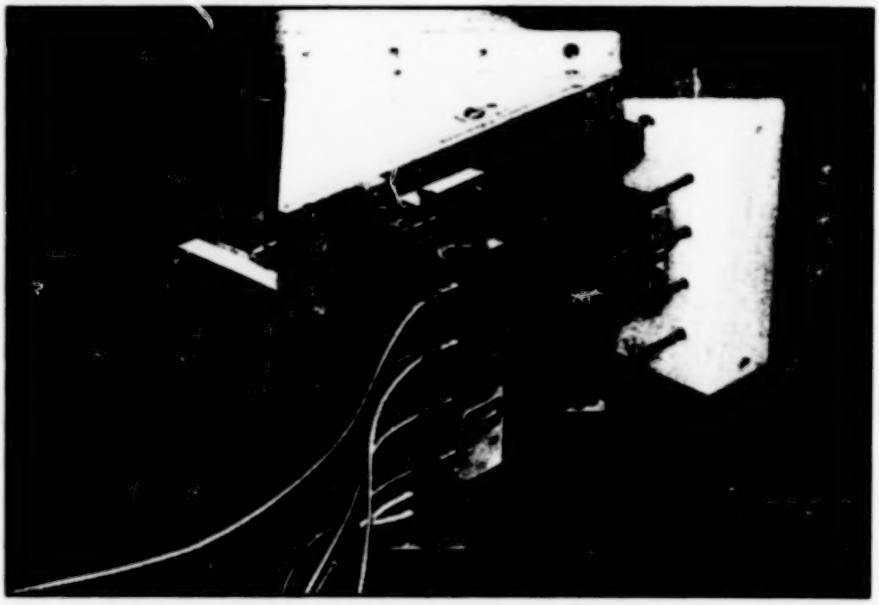

Figure 1. The inside of the Experiment Panel and the Hot-Wire Assembly are depicted in this photograph.

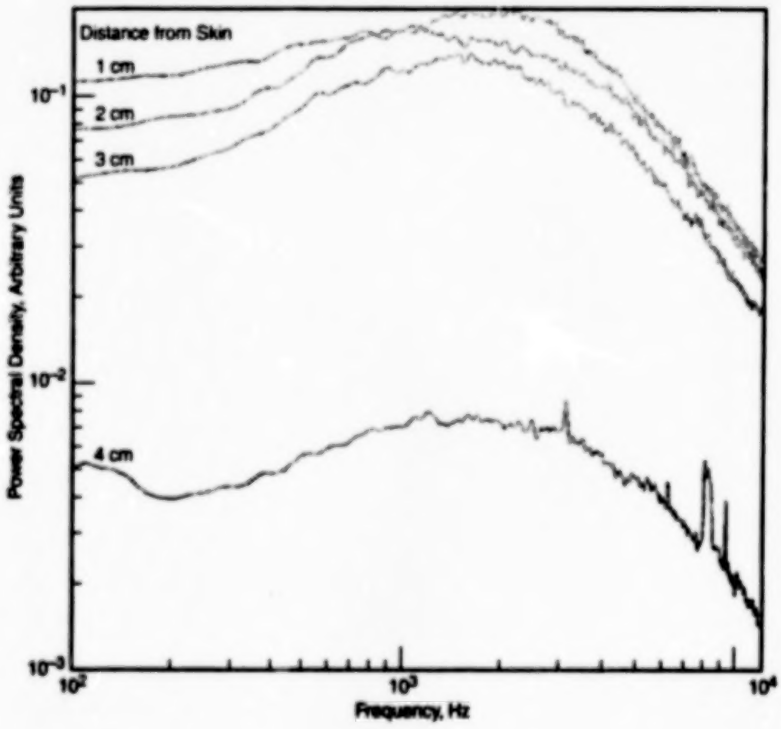

Figure 2. These Power Spectral Densities were computed from hot-wire-anemometer measurements taken at mach 0.9, an altitude of 15,000 ft (=4.6 km), and a local Reynolds number of 2.8×10^7.

The flight-tested CVA system included four hot wires (two wires of 5-μm and two of 10-μm diameter) mounted on probes on the aft panel of the F-15B FTF (see Figure 1). The measurements taken with the wires of each diameter were used to verify the sensitivity and repeatability of

measurements. The hot-wire probes were mounted under the airfoil skin and were extended just prior to collection of data. The probes were extended at an angle of 45° into the boundary-layer flow to distances of 1, 2, 3, and 4 cm from the skin. Data were taken simultaneously for each wire during a time interval of 32 seconds at each flight condition. After collection of data, the probes were retracted. The associated electronic circuits, (including the power supply, CVA subsystem, and data-acquisition subsystem) were installed aboard the FTF.

In the tests, data were taken under various flight conditions ranging between mach 0.6 and mach 1.3 at an altitude of between 15,000 feet (≈4.6 km) and 30,000 feet (≈9.1 km). At the time of reporting the information for this article, analysis of the data was underway. Figure 2 presents a sample of processed data obtained from the flight tests. The raw data were sampled at a rate of 50 kHz and low-pass filtered at frequency of 20 kHz. The plots in Figure 2 show that there was significant turbulence at distances of 1, 2, and 3 cm from the skin. The turbulence was considerably lower at 4 cm from the skin, indicating the edge of the boundary layer. The peaks of the power spectral densities occurred at frequencies between 1,000 and 1,200 Hz. The turbulent energy cascade is clearly indicated, at frequencies above 12 kHz, by approximately constant negative slope at all four boundary-layer locations.

The turbulent data signals were analyzed to determine the degree to which they approximated Gaussian functions. Those obtained at the distances of 1 and 2 cm from the skin were found to be Gaussian, while changes from Gaussian to non-Gaussian were found to occur at distances of 3 and 4 cm.

This work was done by Angela K. Beaver and Donald S. Greer of **Dryden Flight Research Center**. *Further information is contained in a TSP [see page 1].*
DRC-01-15

Improved Alignment Mechanism for Robotic Drilling

The improved design prevents jamming of an alignment key in an incorrect position.

NASA's Jet Propulsion Laboratory, Pasadena, California

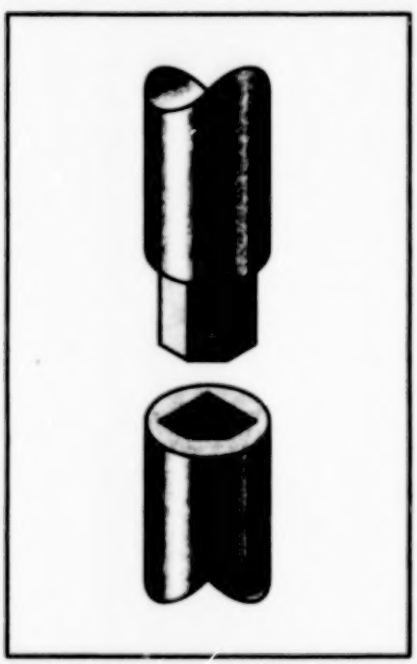

Figure 1. Conventional Mating Schemes incorporating polygonal configuration are susceptible to jamming.

An improved alignment mechanism and mating procedure have been devised for a robotic drilling system in which there is a need to assemble drill stem rods for sampling soils and rocks on a distant planet or asteroid. This mechanism is applicable to systems requiring positive axial alignment between segments. Similar mechanisms could be used on Earth, not only for assembling long drills but also for any system where a series of rods must be robotically assembled, such as in truss construction.

Conventional robotically actuated drill-stem segmenting systems use alignment keys that often feature polygonal protrusions. Figure 1 shows a conceptual example. These mechanisms, while ensuring correct rotational alignment, are susceptible to jamming in a misaligned position. To prevent such jamming, complex control systems must be implemented that can provide fairly accurate alignment between the stem segments prior to any mechanical engagement. Additional control must also be implemented to deal with the possibility that jamming occurs.

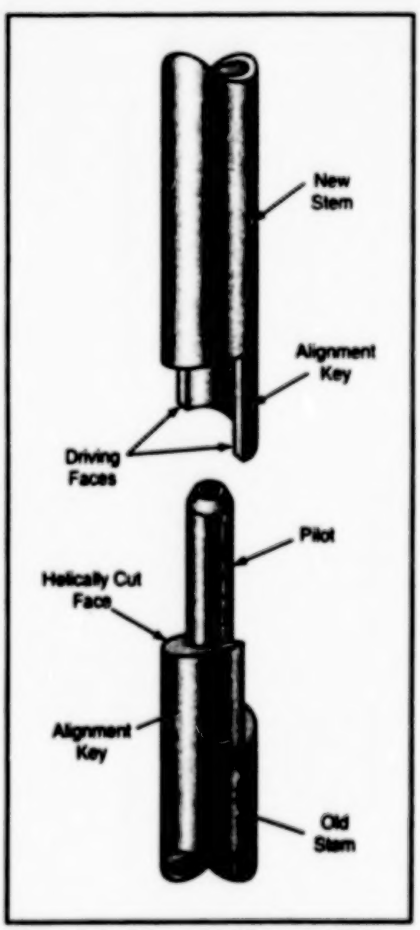

Figure 2. An Improved Alignment Mechanism does not require rotational alignment prior to engagement.

The improved alignment mechanism and mating procedure preclude any chance of jamming during assembly. The mechanism also does not require rotational alignment prior to engagement. The interface is a "half dog clutch," a mating scheme where two half cylinders are mated together (see Figure 2). However, the alignment keys are cut so as to produce a helical face. These keys are used for rotational alignment as well as torque transfer between segments. In the current implementation, an additional pilot is used to ensure axial alignment, but this feature may not always be necessary. The following steps are used to mate the segments:

1. The segments to be aligned are moved toward each other until contact between them is sensed. It may be beneficial to slowly rotate one of the rods in the direction opposite that of a flat cut that is part of the alignment key to help ensure that the helical faces of the dogs contact first.
2. The rods are moved apart to a distance that is fraction of the height of the alignment key.
3. The rods are re-engaged by simultaneous rotation and translation in such a way that the tip of the alignment key travels parallel to the helical alignment-key surface. This motion ensures that

next contact will be between driving faces, at which time positive axial alignment is achieved.

4. The axial-rotational movement can continue until full engagement of the segments is achieved and detected, assuming that one segment is held freely so that the other may drive it.

Note that for this entire process only two simple sensory inputs are required. At no point must the control system know the rotational position of either segment.

This work was done by Benjamin Dolgin and Stephen Askins of Caltech for **NASA's Jet Propulsion Laboratory.** *Further information is contained in a TSP [see page 1].*
NPO-21164

Measuring Volume of Incompressible Liquid in a Rigid Tank

The measurement is unaffected by the shape of the liquid or tank.

NASA's Jet Propulsion Laboratory, Pasadena, California

A technique for measuring the volume of an incompressible liquid in a rigid tank involves measurement of the total volume of gas in those parts of the tank not occupied by the liquid. The volume of liquid is then computed by subtracting V from the total volume of the tank and the associated plumbing.

Unlike liquid-level-measuring techniques, this technique works whether or not a gravitational field is present and is unaffected by the shape of the liquid or tank. Even if bubbles of gas are present in the liquid or if the liquid has broken up into separate globules or pools, the measurement of the total volume of gas is unaffected.

The pressure in the tank is measured while the total volume of the tank is varied by use of a piston or bellows (see figure). It is assumed that the gas is a noncondensible ideal gas, that the alternating compression and decompression of gas is adiabatic, and that the variation in volume is a small fraction of the total volume of gas. Under these assumptions, the total volume (V) of gas in the tank is given by $V = -\gamma P(\Delta V/\Delta P)$, where γ is the specific heat of the gas at constant pressure ÷ the specific heat of the gas at constant volume, P is the pressure, ΔV is the change in volume, and ΔP is the change in pressure that accompanies the change in volume. In a demonstration of this technique, the volume of water in a 94-liter tank was determined within 1 liter.

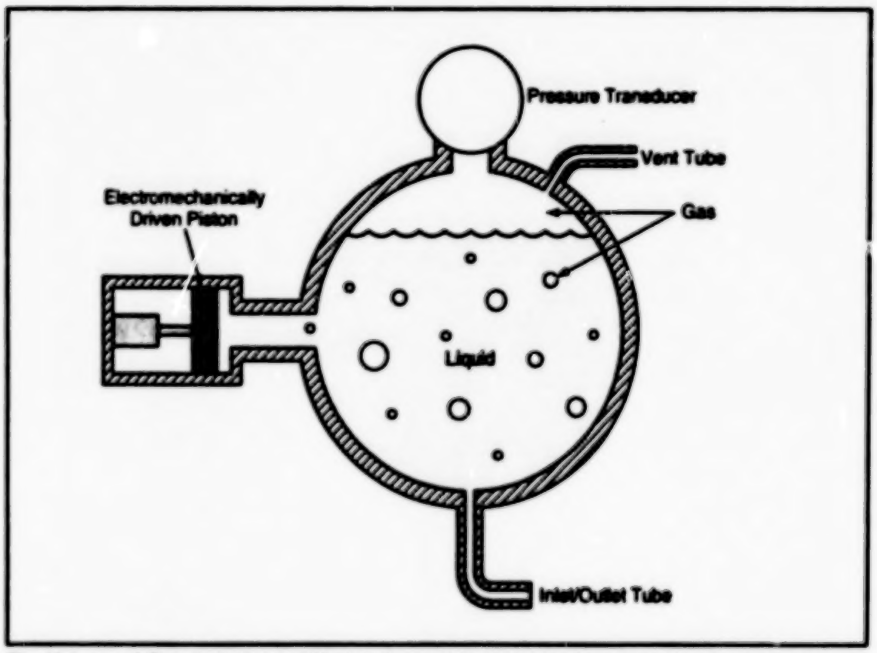

The Volume of Gas (including bubbles) in the tank is determined by measuring the small change in pressure that accompanies a small change in volume. The volume of liquid is then computed by subtracting the volume of gas from the total volume of the tank and plumbing.

This work was done by Frank T. Hartley of Caltech for **NASA's Jet Propulsion Laboratory.** *Further information is contained in a TSP [see page 1].*
NPO-19211

Books and Reports

Algorithms for Collision-Avoidant Formation Flying

A report discusses algorithms for real-time planning of translation paths of multiple spacecraft flying in formation. The algorithm takes account of requirements to avoid collisions while operating within resource constraints (e.g., not calling for an acceleration greater than maximum possible) and striving for optimality (e.g., completing a change of formation in minimum time or at minimum energy cost). The optimality/collision-avoidance problem is formulated as a parameter-optimization problem, in which the translation path of each spacecraft is parameterized by polynomial functions of time. It is shown that this parameterization is the key to the solution of the parameter-optimization problem in that it enables decoupling of the collision-avoidance and acceleration-limit constraints, thereby making it possible to solve the problem in two stages. In the first stage, one constructs feasible paths that satisfy only the collision-avoidance constraints subject to certain optimality criteria. It is shown that the acceleration-limit constraints can be imposed *a posteriori* to compute the required maneuver duration such that at least one acceleration component is saturated. This also enables construction of paths that require minimum time in the class of solutions being considered.

This work was done by Gurkirpal Singh and Fred Hadaegh of Caltech for **NASA's Jet Propulsion Laboratory.** *To obtain a copy of the report, "Collision Avoidance Guidance for Formation-Flying Applications," see TSP's [page 1].*

This software is available for commercial licensing. Please contact Don Hart of the California Institute of Technology at (818) 393-3425. Refer to NPO-30332.

Improvements in a Piezoelectrically Actuated Microvalve

A report discusses the continuing development of a normally closed, piezoelectrically actuated valve fabricated mostly by micromachining of silicon. The design and operation of the microvalve as described in the instant report are basically the same as those of the version described in "Improved Piezoelectrically Actuated Microvalve" (NPO-30158), *NASA Tech Briefs*, Vol. 26, No. 1 (January 2002), page 29. Major elements of design described in both the instant report and the cited prior article include (1) a pressure-aided sealing configuration that contributes to the desired normally-closed mode of operation and (2) knife-edge sealing rings that reduce susceptibility to trapping of particles and the consequent leakage. The report also presents additional information concerning details of design and fabrication, including, notably, additional justification for knife-edge (in contradistinction to blunt-cross-section) sealing rings: The knife-edge sealing rings provide greater sealing pressure at a given sealing force, thereby reducing the leak rate and even making it possible to achieve an adequate seal with a hard seat. A potential additional advantage of the knife-edge/hard-seat design is that contact pressures may be high enough to crush contaminant particles, thereby reducing the leakage attributable to contaminants.

This work was done by Eui-Hyeok Yang, Larry Wild, and Nishant Rohatgi of Caltech for **NASA's Jet Propulsion Laboratory**. *To obtain a copy of the report, "A micro valve for high pressure applications," see TSP's [page 1].*

In accordance with Public Law 96-517, the contractor has elected to retain title to this invention. Inquiries concerning rights for its commercial use should be addressed to

Intellectual Assets Office
JPL
Mail Stop 202-233
4800 Oak Grove Drive
Pasadena, CA 91109
(818) 354-2240
E-mail: ipgroup@jpl.nasa.gov

Refer to NPO-30338, volume and number of this NASA Tech Briefs *issue, and the page number.*

Low-Energy Transfer From Near-Earth to Near-Moon Orbit

A report presents a theoretical approach to designing a low-energy transfer of a spacecraft from an orbit around the Earth to ballistic capture into an orbit around the Moon. The approach is based partly on the one presented in "Low-Energy Interplanetary Transfers Using Lagrangian Points" (NPO-20377), *NASA Tech Briefs*, Vol. 23, No. 11 (November 1999), page 22. The approach involves consideration of the stable and unstable manifolds of the periodic orbits around the Lagrangian points L1 and L2 of the Sun/Earth and Earth/Moon systems. (The Lagrangian points are five points, located in the orbital plane of two massive bodies, where a much less massive body can remain in equilibrium relative to the massive bodies.) To generate a transfer trajectory, one uses the intersection of (1) the unstable manifold of a periodic orbit about the Sun-Earth L1 or L2 with (2) the stable manifold of a periodic orbit about the Earth-Moon L2. This intersection is generated by a Poincaré section. The different regions within the Poincaré section all have different dynamical properties. By picking points in the correct region, one can generate a transfer from orbit around the Earth to capture into a highly elliptical orbit around the Moon.

This work was done by Martin Lo, Jerrold Marsden, Wang S. Koon, and Shane Ross of Caltech for **NASA's Jet Propulsion Laboratory**. *To obtain a copy of the report, "Low Energy Lunar Transfer and Capture," see TSP's [page 1].*

NPO-20936

Machinery

Hardware, Techniques, and Processes

49 Vision-Based Maneuvering and Manipulation by a Mobile Robot

Books and Reports

49 Integrated Colloid Thrusters for Microspacecraft

BLANK PAGE

Vision-Based Maneuvering and Manipulation by a Mobile Robot

Mobility is used to augment limited dexterity.

NASA's Jet Propulsion Laboratory, Pasadena, California

A small mobile robot equipped with a stereoscopic machine vision system and two manipulator arms that have limited degrees of freedom has been given the ability to perform moderately dexterous manipulation autonomously, under control by an onboard computer. The approach taken in this development has been one of formulating vision-based control software to utilize the mobility of the vehicle to compensate for the limitation on the dexterity of the manipulator arms. Although the goal was selected visually, it is tracked onboard using information about its shape; in particular, the target is assumed to be a local elevation maximum (i.e., the highest point within a small patch of area).

The mobile robot in question is Rocky 7 — a prototype "rover"-type vehicle used in research on robotic-vehicle concepts for the exploration of Mars. The mobility system of Rocky 7 is based on a six-wheel-drive rocker-bogey mechanism that includes two steerable front wheels and four nonsteerable back wheels. One of the manipulator arms is equipped with two independently actuated scoops for acquiring samples. Not counting the motions of the scoops, this arm has two degrees of freedom — shoulder roll and a shoulder pitch. The other manipulator arm is a mast on which is mounted a stereoscopic pair of video cameras and that can, if desired, be tipped with a scientific instrument. The mast has three degrees of freedom (shoulder pitch, shoulder roll, and elbow pitch). The mast can be used to position and orient its cameras and/or to place its tip instrument on a target object to acquire a sample or take a reading. Additional stereoscopic pairs of cameras are located at the front and rear ends of the main body of the vehicle.

At the beginning of an operation, one or more target objects a small distance away are selected, and then the robot is commanded to perform autonomously some manipulations that involve the objects. Following the basic approach of using mobility to augment dexterity, the navigation and mobility control subsystems of the vehicle cause the vehicle to maneuver into a position and orientation in which the target lies within the range of one of the manipulators (see figure), and then the manipulator control subsystem causes the manipulator to perform the remaining fine positioning and manipulation.

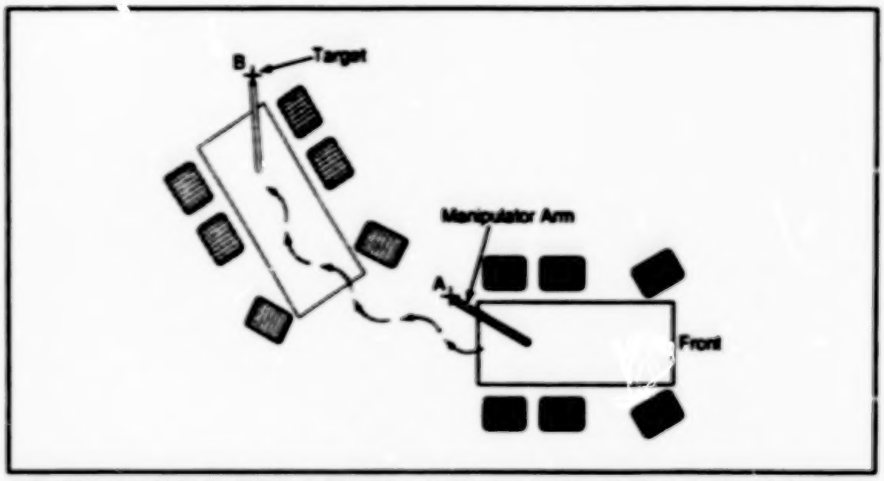

A Six-Wheeled Robotic Vehicle Is Moved — in this case, backward along a series of circular arc segments — while visually tracking the target, so that the manipulator-arm workspace initially at position A can be robustly moved onto the target at position B.

The key to ensuring that the rover reaches its target is to move in small steps, and lock onto the target by automatically tracking its *shape*. The computer processes the image data from the stereoscopic camera pairs into an elevation map of the nearby terrain and locates the target on the elevation map. The computer plans the route of the vehicle across the terrain toward the target, using an approximate kinematical model (assuming flat terrain and no slippage of wheels). At frequent intervals along the route, updated elevation maps are generated from newly acquired stereoscopic-image data, the target is identified on the updated maps, and the planned route is corrected accordingly. Here the *scale-invariant* features (i.e., shape, elevation, and centroids) are tracked: this allows one to track the target even as its image grows dramatically in size during the final approach, a situation that often causes traditional visual servoing techniques to fail. This process of iterative, vision-based refinement of the route continues until the vehicle arrives at the desired location near the target.

Once the vehicle is in the desired position and orientation relative to the target, the designated manipulator arm is lowered toward the target; tactile sensing is used to signal contact with the target or with the ground adjacent to the target. The manipulator arm is then commanded to perform the assigned manipulation. Manipulations that Rocky 7 has performed in demonstrations include grasping several small rocks that were initially at a distance of >1 m and placing an instrument on a boulder that was initially at a distance of >5 m.

This work was done by Mark Maimone, Issa Nesnas, and Hari Das of Caltech for **NASA's Jet Propulsion Laboratory.** *Further information is contained in a TSP* *[see page 1].*

NPO-21011

Books and Reports

Integrated Colloid Thrusters for Microspacecraft

A report proposes the development of a microfabricated, integrated colloid thruster as a prototype of devices for propulsion and control of the attitudes of microspacecraft. (In a colloid thruster, a beam of positively charged, microscopic droplets is extracted electrohydrodynamically from a column of liquid and accelerated electrostatically to produce thrust.) Unlike other electrical thrusters, colloid thrusters are amenable to extreme miniaturization. The volume of the proposed thruster (excluding that of the tank holding the liquid) would be about 1 cm^3. The liquid would be fed by capillary action, eliminating the need for valves. Integrated driver electronic circuitry would operate at a supply potential of 5 V. An embedded lin-

ear electrostatic accelerator would operate in a traveling-wave mode with shaped DC pulses creating the high electric fields needed for acceleration; this aspect of the design would enable the use of accelerator voltage significantly less than the several kV typical of other electric thrusters. The accelerator voltage would be generated by an on-chip transformer and/or a capacitor-and-diode voltage multiplier. The direction of thrust would be controlled electronically through selective activation of accelerator electrodes, eliminating the need for mechanical gimbals.

This work was done by Mohammed Mojarradi, Juergen Mueller, Jay Polk, and Colleen Marrese-Reading of Caltech for NASA's Jet Propulsion Laboratory. To obtain a copy of the report, "A Fully Integrated Micro-Colloid Thruster System for Microspacecraft Applications," see TSP's [page 1].

In accordance with Public Law 96-517, the contractor has elected to retain title to this invention. Inquiries concerning rights for its commercial use should be addressed to

Intellectual Assets Office
JPL
Mail Stop 202-233
4800 Oak Grove Drive
Pasadena, CA 91109
(818) 354-2240
E-mail: ipgroup@jpl.nasa.gov

Refer to NPO-20945, volume and number of this NASA Tech Briefs issue, and the page number.

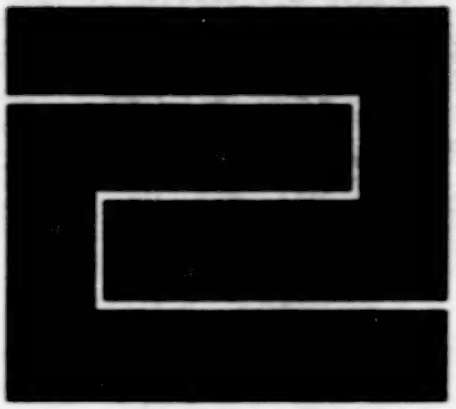

Fabrication Technology

Hardware, Techniques, and Processes

53 Photolithographic Fine Patterning of Difficult-To-Etch Metals

53 Software for Optimized Flattening From 3D to 2D

54 Electron-Beam Welding of Superalloys at High Temperatures

BLANK PAGE

Photolithographic Fine Patterning of Difficult-To-Etch Metals

Copper is used as a liftoff material.

John H. Glenn Research Center, Cleveland, Ohio

A process that includes photolithography, liftoff, etching, and sputter deposition has been developed to enable the fabrication of thin, finely patterned layers of gold, platinum, and other difficult-to-etch materials in advanced miniature sensors and associated electronic circuitry. Heretofore, photolithography has been used in conjunction with liftoff and etching to produce finely detailed structures in easy-to-etch materials. The present process is needed because conventional photolithography cannot be used to pattern difficult-to-etch materials and the alternative processes heretofore available for patterning difficult-to-etch materials are limited to spatial resolution of about 0.005 in. (≈0.13 mm) or coarser.

The process (see figure) includes some new steps plus some steps from prior processes that are used with modifications and in a different sequence. The sequence is the following:

1. Copper is deposited over an entire face of a substrate of suitable material (e.g., alumina). If the substrate material is one to which copper does not adhere well, aluminum or nickel can be used instead of copper. The thickness of the copper (or aluminum or nickel, as the case may be) should be made roughly three times that of the final desired difficult-to-etch metal layer.
2. The copper is covered with positive photoresist.
3. The photoresist is soft-baked.
4. The photoresist is exposed through a photomask in the desired pattern.
5. The photoresist is developed.
6. It is hard baked at 110 °C for 30 minutes.
7. The entire workpiece is washed with a half-and-half mixture of nitric acid and water to remove the copper from the regions in which the difficult-to-etch metal is to be deposited. This removal of copper is facilitated by a slight undercutting of the photoresist.

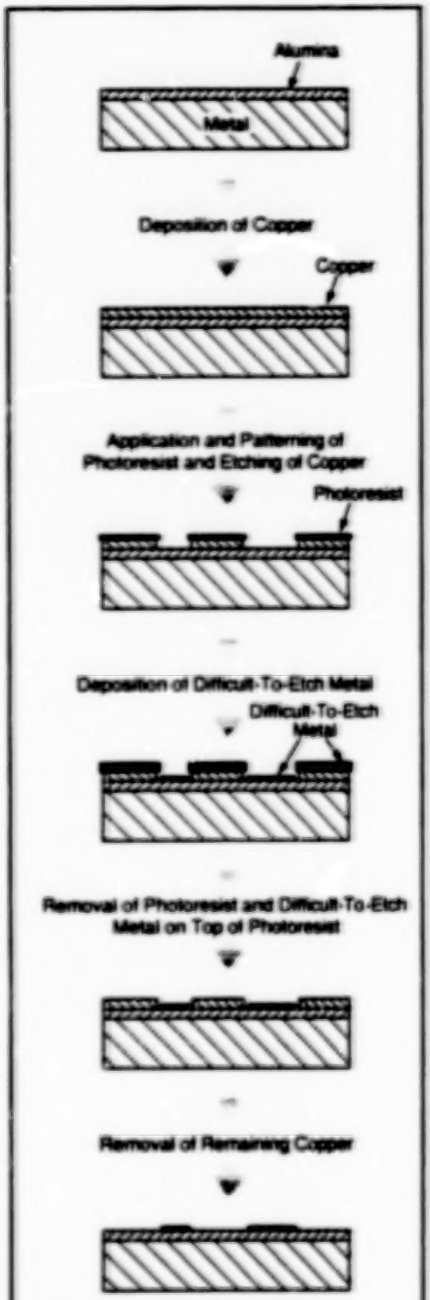

A Mask for Sputter Deposition of a difficult-to-etch metal is made of copper with overhanging photoresist. The photoresist and copper are removed after the deposition.

The most significant aspect of this process is the use of copper as the liftoff material. Partly because of the rapidity with which copper is etched, it is possible to control the amount of undercutting of the photoresist and to ensure that the undercutting occurs uniformly and cleanly. Undercutting is very important to the success of this process: it expedites removal of unwanted material later in the process and increases the sharpness of the final pattern of difficult-to-etch metal.

8. The substrate holder is precooled to 10 °C before the piece is loaded into the sputtering system.
9. The difficult-to-etch metal is sputter-deposited at a relatively low power density (0.14 W/cm^2) over the entire substrate. In the regions from which the copper and photoresist were previously removed, difficult-to-etch metal becomes deposited directly onto the substrate. During the deposition of the difficult-to-etch metal, the substrate is cooled to prevent the carbonization of the photoresist; this is necessary because carbonization would make the subsequent removal of the photoresist more difficult.
10. The workpiece is washed with acetone to remove all the photoresist plus the portion of difficult-to-etch metal deposited on top of the photoresist.
11. The workpiece is washed with the nitric acid/water mixture to etch away all the remaining copper, leaving the desired difficult-to-etch metal pattern.

This work was done by Charles A. Blaha of Akima Corp. for **Glenn Research Center.** *Further information is contained in a TSP [see page 1].*

Inquiries concerning rights for the commercial use of this invention should be addressed to NASA Glenn Research Center, Commercial Technology Office, Attn: Steve Fedor, Mail Stop 4–8, 21000 Brookpark Road, Cleveland, Ohio 44135. Refer to LEW-17079.

Software for Optimized Flattening From 3D to 2D

Manufacturing considerations can be taken into account in designing minimally wasteful 2D patterns.

John H. Glenn Research Center, Cleveland, Ohio

A computer program offers enhanced capabilities for calculating two-dimensional (2D) patterns needed to construct specified three-dimensional (3D) surfaces to within acceptably close approximations, with minimal waste of sheet material. Examples of complexly shaped sheet-material items that could be designed by use of this program include aircraft fuselages, hulls of

ships, clothing, and automotive bodies.

This program offers two advantages over the flattening subprograms of prior computer-aided-design, computer-aided manufacturing (CAD-CAM) programs:

- The program utilizes all available pertinent information, including not only information on the desired 3D shape but also information about the manufacturing process in which the two-dimensional pattern(s) would be formed into the 3D surface. The more information about the 3D surface and the manufacturing process that is available, the better can be the match between the 3D surface and the 2D pattern(s) used to construct it.
- The program affords options that enable the user to define and build a method of solution based on the unique characteristics of, and the available data about, the 3D surface. In particular, the program can implement any or all of four independent procedures, and for each procedure there is a choice of several algorithms. This array of options enables the user to integrate any available pertinent information into the solution via at least one procedure.

In the event that the desired 3D surface is one that can be fabricated by bending only (such a surface is termed "developable" in the art) then procedures 1 and 2 are the only ones needed. However, if in-plane deformations (stretching or shrinking) are needed, or if there is a need to bend any portion of sheet material upon itself to form multiple layers, then procedure 3 or procedures 3 and 4 must also be used.

In procedure 1, boundaries that divide a 3D surface into regions are placed into a plane. Because the algorithms defining these boundaries can be chosen from a library of algorithms, these boundaries serve as initial conditions which help define a unique flattening process. The placement of these boundaries depends on several factors unique to the 3D surface. One factor, which can be controlled by placement of the boundaries, is to allow or not allow distortions to move from one 2D region into another 2D region. Also, the user might want to satisfy some general 2D outer-boundary constraints, which can be addressed only at the boundary-placement level. Some 3D surface boundaries cannot be placed directly into the 2D plane by procedure 1. Such a boundary is not amenable to placement by use of one or two algorithms alone; instead, it is necessary to "grow" the boundary into the 2D plane during the execution of procedure(s) 2, 3, and/or 4.

In procedure 2, 3D cell walls are placed into the plane, such that the lengths of the 3D arcs of each cell wall are preserved in the plane. At this point, the program is working in the 2D plane but is using information which geometrically defines the corresponding 3D surface triangle. After procedure 2 has been performed at the local level on an individual cell, the user is then given the option of using either procedure 3 or procedures 3 and 4. These two procedures involve the relationship between the area and geometry of a 3D cell and the area and geometry of the corresponding recently formed 2D cell. In particular, if the user knows there was a local expansion, contraction, or folding of the 2D sheet during the manufacturing process, then procedure 3 or procedures 3 and 4 must be used. These procedures modify the local 2D cell by incorporating, into the 2D cell, the inverse stresses and strains inherent in the manufacturing process of forming a 3D surface from a 2D surface. Procedure 4 is used and coupled to procedure 3 if the expansion or contraction factors are associated with preferred directions.

Another important element of the program logic is the coupling of procedure 2 directly to procedure 3 by feeding the geometric solution of procedure 2 into procedure 3. The geometric solution from procedure 2 serves as an initial geometry from which procedure 3 (or 3 and 4) can geometrically and algebraically iterate. During this iteration, the 3D cell is transformed from a predefined 3D cell geometry to a 2D cell geometry which satisfies input data defining the manufacturing process.

This work was done by Bruce M. Auer of **Glenn Research Center**. *Further information is contained in a TSP (see page 1).*

Inquiries concerning rights for the commercial use of this invention should be addressed to NASA Glenn Research Center, Commercial Technology Office, Attn: Steve Fedor, Mail Stop 4–8, 21000 Brookpark Road, Cleveland, Ohio 44135. Refer to LEW-17029.

Electron-Beam Welding of Superalloys at High Temperatures

Strain age cracks can be prevented.

John H. Glenn Research Center, Cleveland, Ohio

Electron-beam welding at high temperatures has been found to be a suitable process for joining structural components made by casting certain superalloys. This process can be used in the fabrication of superalloy parts that must withstand high operating temperatures. Examples of such parts include exhaust ducts of advanced aerospace engines and end caps on turbine buckets.

The superalloys in question are γ'-strengthened nickel-base alloys that contain either >3 weight percent Al or >5 percent Ti. Strain age cracks form in such alloys upon cooling after welding or on subsequent reheating to aging temperatures. The cracks result from a combination of residual stresses produced during welding and aging cycles. Heretofore, the formation of the strain age cracks has made it impossible to utilize these superalloys to make welded structures.

The development of the present process brought electron-beam welding together with vacuum heat treatment to provide a new industrial capability. Electron-beam welding has long been used to produce structural weldments in a wide variety of alloys, but, heretofore, has not been successful for welding nickel-base superalloy structures. Nickel-base superalloys are frequently heat-treated in vacuum furnaces to impart the very properties for which they were selected.

In the present process, a heat-treating furnace is placed in the vacuum chamber of an electron-beam welding machine. A superalloy structure to be welded is placed in the furnace. Prior to and during welding, the furnace is used to heat the entire superalloy structure to a temperature at or near the solution temperature of the alloy. Maintaining the entire structure at this temperature reduces or eliminates the thermal stresses produced by the differential thermal expansion during welding. Further, maintaining this temperature for a while after welding affords some relief of solidification stresses, thereby helping to prevent subsequent strain age cracking. The structure can then be cooled rapidly and later aged or can be aged during the cooling cycle after welding has been completed. An additional advantage

is that the reduction in thermal stress prevents the formation of liquation cracks in the heat-affected zones of the welds.

This work was done by Thomas J. Kelly of General Electric Co. for **Glenn Research Center**. *Further information is contained in a TSP [see page 1].*

Inquiries concerning rights for the commercial use of this invention should be addressed to NASA Glenn Research Center, Commercial Technology Office, Attn: Steve Fedor, Mail Stop 4–8, 21000 Brookpark Road, Cleveland, Ohio 44135. Refer to LEW-16686.

BLANK PAGE

Mathematics and Information Sciences

Hardware, Techniques, and Processes

59 Compensating for Motion Errors in UWB SA[illegible]ata

59 Making Digital Composite Images for Technical Illustration

BLANK PAGE

Compensating for Motion Errors in UWB SAR Data

Processing is implemented in two stages by a computationally efficient algorithm.

NASA's Jet Propulsion Laboratory, Pasadena, California

A method of processing data acquired by ultra-wide-band (UWB) synthetic-aperture radar (SAR) provides for suppression of those errors that are caused by the undesired relative motion of the radar platform and the targets. This method involves, among other things, processing of data in the wave-number or frequency domain and the application of motion compensation as a function of the positions of a target relative to the radar platform.

The need for this method arises because of two sources of complication in UWB SAR that are not present in narrow-band SAR. One source of complication is that the prior commonly used SAR motion-compensation algorithm depends upon the Doppler shift of a well-defined radar-signal frequency, but the signal frequency in UWB radar is not well defined. The other complication is that the prior motion-compensation algorithm depends on azimuthal narrowness of the radar beam, but in UWB SAR, the requirement to make the range and azimuth resolutions approximately equal translates to a requirement that the radar beam be azimuthally wide (typical width of the order of a radian).

In a wide-beam SAR system, the key dilemma in properly compensating for motion is that one needs to track the location of each target on an SAR strip map, but the locations of the targets are not known from the outset. The present method addresses this dilemma. The method involves two stages of processing (see figure).

In the first stage, a strip parallel to the flight track is processed and targets are motion compensated, assuming that they are located in the antenna fan beam plane.

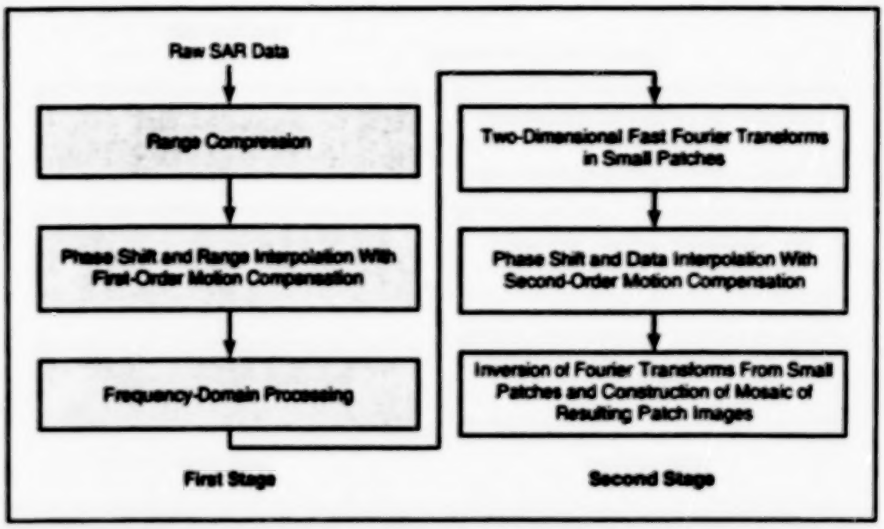

Motion Compensation to first order is effected for a data strip, then refined to second order over small overlapping constituent patches. A motion-compensated image of the large patch is then constructed as a mosaic of the images of the smaller patches.

Following the first-order motion compensation, a frequency-domain SAR processing algorithm is applied. The motion compensation for targets in off-boresight directions is not correct, but the motion compensation for the target(s) in the nominal center of the beam is correct. This stage of processing ensures that target impulse responses are located correctly geometrically, albeit insufficiently focused.

In the second stage of processing, the data strip is divided into overlapping small patches and it is pretended that the target(s) in each small patch lie at the center of the patch. The data processed in stage 1 are reprocessed within each small patch to refine the motion compensation. This reprocessing includes second-order motion compensation that takes the form of frequency and phase shifts applied to the partially motion-compensated UWB SAR data. Inasmuch as the motion compensation is perfect only at the center of each small patch, the smaller the patches, the better the motion-compensation performance. For the sake of computational efficiency, the two-stage processing algorithm has been formulated such that the reprocessing in small patches is much less computationally demanding than is the processing of the wide area patch, such that it is computationally affordable to reprocess many small patches.

This work was done by Soren Madsen of Caltech for **NASA's Jet Propulsion Laboratory**. *Further information is contained in a TSP [see page 1].*

NPO-21096

Making Digital Composite Images for Technical Illustration

Drawings of facilities to be modified can be made in less time.

John F. Kennedy Space Center, Florida

A method of generating three-dimensional composite digital images can serve multiple purposes in technical illustration. The method was devised to accelerate and facilitate the design of new electric lights and receptacles for large buildings, and can just as well be applied to the design, redesign, and analysis of other buildings and equipment.

In the original application that motivated the development of this method, it would have taken an excessively long time to make traditional-style drawings by the traditional method, because of the complexity of the facilities. Accordingly, a major element of the method is that one makes detailed three-dimensional drawings of only those parts of the facilities and equipment that are to be modified. Data on the parts not to be modified are acquired by photographing the facilities in their present state by use of a digital camera and, if necessary, retouching the digital photographs by use of commercial software developed for that purpose.

Computer-aided-design (CAD) software is used to generate three-dimensional computational models from the new draw-

ing data. Materials are assigned to the surfaces of the models. The models are rotated to match the perspective and lighting of the digital photographs, and are then composed onto the photographs. If necessary, hidden-line isometric profiles are created from the three-dimensional models and rendered as details in drawings. The models are created only once and are reused in different views; they can also be reused on different projects.

This method greatly reduces the amount of time needed to make drawings for modifications of facilities. In this method, unlike in the traditional method, little or no time is spent in research of prior drawings or in measuring dimensions. The composite images generated by this method have higher levels of detail and are easier to understand, relative to traditional drawings. An additional and unobvious advantage afforded by these images is that they can reveal conflicts in original designs of facilities and equipment. The composite images can be printed in color, generated as dozens of different file formats (including portable document format (.pdf)) that can be transmitted by electronic mail, incorporated into CAD drawings, or documents generated by word-processing software, and/or attached to MAXIMO work orders.

This work was done by Arlene S. Reese, Thomas Bigelow, and Robert C. Kemmerling of United Space Alliance for **Kennedy Space Center.**
KSC-12288

Life Sciences

Hardware, Techniques, and Processes

63 Petri-Dish Spreaders Sterilized by Electrical Heating

64 Quantifying Microbial Diversity Through Dilution/Extinction

BLANK PAGE

Petri-Dish Spreaders Sterilized by Electrical Heating

Sterilization is faster, easier, and less expensive than it is for conventional glass spreaders.

Lyndon B. Johnson Space Center, Houston, Texas

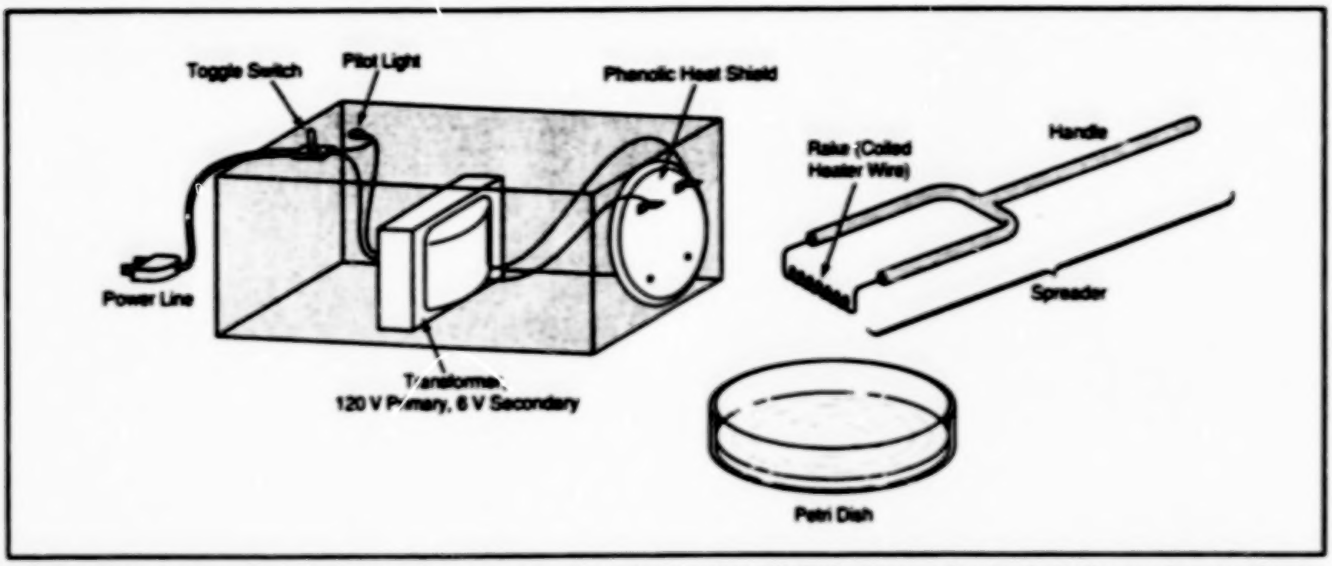

A Rake Made of Coiled Wire is heated by placing the ends of the wire in contact with the 6-volt secondary terminals of a step-down transformer. The heating sterilizes the rake, so that it can be used to spread micro-organisms over a petri dish.

An improved method of sterilizing petri-dish spreaders and a spreader design to implement the method have been developed. In comparison with the conventional methods of sterilizing petri-dish spreaders, the improved method is expected to prove easier, safer, less time-consuming, and less costly, and to require less laboratory space. This improved method could be used in microbiological investigations in microgravity (e.g., aboard the International Space Station) or in normal Earth gravity (e.g., in government and clinical laboratories and research institutions). Particularly, when used in spaceflight, the improved method will prove safer than the traditional flame sterilization method.

The prior art in the design, use, and sterilization of petri-dish spreaders is relatively straightforward. A conventional petri-dish spreader is a glass rod bent like a hockey stick. The longer straight segment of the rod is used as a handle, while the shorter straight segment is used to spread a suspension of microorganisms with a small volume (typically 0.1-mL) evenly over the surface of the growth medium in a petri dish. After a suitable incubation time, colonies of the microbes grow on the surface of the medium. Provided that a known volume of a microbial suspension is spread evenly over the medium, an accurate count can be made, and the types of organisms in the suspension can be identified. If the suspension is not spread correctly, the growing colonies converge and become so crowded that it is hard to see the boundaries between them.

Each time a suspension of microorganisms is spread over a different dish, a sterile glass spreader must be used. A spreader that was used on another dish can be reused if it is dipped into 95-percent ethyl alcohol and the alcohol is then ignited with a flame to sterilize the spreader. If multiple dishes are to be inoculated and insufficient time is available for sterilization of a single spreader between dishes, then multiple sterile spreaders must be prepared in advance, and considerable laboratory space must be allocated for storing them. Moreover, the use of alcohol and an open flame to sterilize spreaders introduces a fire hazard.

In the improved method, the spreader comprises a forked handle and a rake made of a coil of chromel electrical-resistance heater wire (see figure) that draws a current of 3 A when a potential of 6 V is applied. All that one need do to sterilize the rake is to place the end terminals of the wire in contact with the output terminals of a 6-V power source, which can be the secondary terminals of a 120-to-6-V step-down transformer. In this method, one does not attempt to sterilize the entire spreader; only the rake is sterilized. Tests have shown that the rake becomes heated to sterilizing temperature within only 2 to 3 seconds of heating at 6 V. After electrical heating, the rake can be cooled quickly on a damp sterile pad and is then ready to use. The sterility of the spreader in this improved method has been verified by extensive testing involving spreading on sterile media after spreading 0.1 mL of a bacterial solution on a petri dish.

The improved method has proved to be very reliable. Although it involves heat, this method, unlike the flame sterilization method, does not involve either alcohol or an open flame, and thus introduces less of a fire hazard. Because this method makes it unnecessary to use multiple presterilized glass spreaders, it reduces (relative to the flame sterilization method) the amount of storage space needed. Because sterilization and cooling before each use take only a few seconds in this method, preparation time is reduced, relative to that of the flame sterilization method. A further advantage of this method is that, because of its simplicity, little (if any) maintenance is needed.

This work was done by Duane Pierson of **Johnson Space Center** *and Thomas C. Moline of KRUG Life Sciences.*
MSC-22903

Quantifying Microbial Diversity Through Dilution/Extinction

A method of relatively easily, rapidly, and inexpensively quantifying the structural diversity of a multiple-species community of micro-organisms is based on the rate of extinction of phenotypic traits across a dilution gradient of a sample of the community. In this context, the concept of structural diversity encompasses the number (richness) and distribution (evenness) of separate or interacting biological entities responsible for given functions within the overall set of functions performed by the community. It is assumed that the rate of loss of character (as measured through testing for a given function) from the community upon dilution/extinction is proportional to the diversity of biological entities in the community. This assumption should be true as long as the average metabolic versatility of individuals (the width of a nutritional niche) does not increase with structural diversity. Inasmuch as most experimental evidence suggests that the widths of nutritional niches decrease with increasing diversity, the assumption appears valid. In experiments performed to evaluate the method, the nonlinear relationship between the number of positive tests and the density of cells across a dilution series was successfully fit to a rectangular hyperbola, yielding regression variables related to the structural diversity of the sample.

This work was done by Jay Garland of Dynamac Corp. and R. Michael Lehman of Bechtel BWXT, LLC for **Kennedy Space Center.**

KSC-12226

END

11-5-02